Barrier-Function Adaptive Finite-Time Trajectory Tracking Controls for Cyber Resilience in Smart Grids under an Electricity Market Environment

Seyed Hossein Rouhani, *Member*, *IEEE*, Chun-Lien Su, *Senior Member*, *IEEE*, Saleh Mobayen, *Senior Member*, *IEEE* Mostafa Esmaeili Shayan, Mohammad Hassan Khooban, *Senior Member*, *IEEE*, Mahmoud Elsisi, *Senior Member*, *IEEE*

***Abstract*- The advancement and proliferation of digitalization and communication infrastructure have facilitated the rise of real-time bidding markets in smart grids. In these dynamic markets, energy distribution companies and power-generating companies interact to establish energy exchange contracts based on offered prices. However, the fluctuation in power flow resulting from contract changes within the real-time bidding market introduces a potential vulnerability that malicious attackers can exploit to launch successful stealthy attacks. To enhance the smart grid resiliency against cyber-attack in the power market bidding environment, a new barrier-function adaptive finite-time trajectory tracking control is proposed in this paper. The developed controller is utilized to actively counteract and mitigate potential cyber-attacks to ensure their rejection and prevention. The stability analysis convincingly demonstrates the rapid convergence of system states within a finite time frame, empowering the system to effectively reject cyber-attacks in real-time. Test results of an IEEE test systems considering governor dead bound nonlinearity and communication time delay are presented and compared with those obtained from other methods to ensure and demonstrate the performance of proposed method. The Speedgoat real-time target machine, along with Simulink real-time, validates the effectiveness of the proposed method.**

***Index Terms*- Finite-Time Tracking, Barrier-Function, Second Order Sliding Mode, Time Delay, Cyber-Attack Detection and Prevention.**

NOMENCLATURE

GENCO	Generation Company
DISCO	Distribution Company
ICT	Information and Communications Technology
ISOs	Independent System Operators
SCADA	Supervisory Control and Data Acquisition
AGC	Automatic Generation Control
SMC	Sliding mode Control
EP	Equilibrium Point
DPM	DISCOs participation matrix
PID	Proportional-integral-derivative
ACE	Area Control Error
ACE_d	ACE signal in the deregulated environment
cpf_{ij}	Contract between GENCO *i* and DISCO *j*
apf	ACE participation factor
$\Delta P_{tie,i}$	Deviation of the active power transferred from area *i*
$\Delta\omega_i$	Angular frequency deviation in area *i*
$\beta_{d,i}$	Frequency bias coefficient in area *i*
$D_{p,i}$	Load-damping factor
$R_{G,i}$	Speed droop constant
$\Delta P_{L,j}$	Demanded load by DISCO *j*
$\Delta P_{mech,k,i}$	Deviation of generated mechanical power for the k^{th} GENCO in area *i*
H_i	Inertia in area *i*
T_{ij}	Synchronizing power coefficient between areas *i* and *j*
$T_{t,k,i}$	Turbine time constant for the k^{th} GENCO in area *i*
$\Delta P_{valve,k,i}$	Deviation of valve of the governor for the k^{th} GENCO in area *i*
T_G	Time constant of a governor
$T_{G,k,i}$	Time constant of a governor for the k^{th} GENCO in area *i*
$R_{G,k,i}$	Speed droop constant for the k^{th} GENCO in area *i*
u_i	System inputs which is the controller output.
$f_n(.)$	Nonlinearity.
$fdi_{o,i}$	Effect of the cyber-attack in area *i*.
$fdi_{s,i}$	Effect of the cyber-attack in area *i*.
X_i	System states vector for area *i*
x	System state
i	The i^{th} controlling area
τ	Delay
$A_{n,i}$	System matric
$B_{n,i}$	Coefficient matrix for system input
B_{mb}	Coefficient matrix for deregulated bidding market
B_{lv}	Coefficient matrix for load variation
$B_{fdi,s}$	Coefficient matrix for the cyber-attack effect on the bidding market
$C_{n,i}$	Coefficient matrix for system output
$D_{mb,i}$	Coefficient matrix for direct input to output from the bidding market
u_{lv}	Unknown input due to the load variation
u_{mbs}	Input from the bidding market
$u_{mbo,i}$	Direct input to output from the bidding market
$y_{n,i}$	System outputs
$x_{n,j}$	Interconnected area states
$A_{n,ij}$	Coefficient matrix depicting relation between area *i* and *j*

S. H. Rouhani, and C. L. Su are with the Department of Electrical Engineering, National Kaohsiung University of Science and Technology, Kaohsiung City 807618, Taiwan (Email: hosseinrouhani@nkust.edu.tw; cls@nkust.edu.tw; mahmoudelsisi@nkust.edu.tw). S. Mobayen is with the Graduate School of Intelligent Data Science, National Yunlin University of Science and Technology, Douliou, Yunlin 640301, Taiwan (Email: mobayens@yuntech.edu.tw). M. Esmaeili Shayan is with the Department of Mechanical, Chemical and Materials Engineering, University of Cagliari, Via Marengo, 2, 09123 Cagliari, Italy (Email: mostafa.esmaeili@unica.it). M. H. Khooban is with the Department of Electrical and Computer Engineering, Aarhus University, Aarhus, Denmark (Email: khooban@ece.au.dk). M. Elsisi is with the Department of Electrical Engineering, National Kaohsiung University of Science and Technology, Kaohsiung City 807618, Taiwan and the Department of Electrical Engineering, Faculty of Engineering (Shoubra), Benha University, Cairo 11629, Egypt. (E-mail: mahmoudelsisi@ nkust.edu.tw).
*Corresponding authors: C. L. Su (cls@nkust.edu.tw), S. Mobayen

$E_{fdi,o}$	Coefficient matrix related to under attack output matrix
n	Number of states
nc	Number of interconnected system input from secondary controller
nlv	Number of system input from the load variation
$nmbs$	Number of system input from power bidding market
$nmbo$	Number of the direct input to output from power bidding market
ns	Number of the under-attack states
p	Number of the system output
no	Number of the output under attack
T_{or}	Orthogonal decomposition matrix
$y_{n,1}(t)$	Non attack output
$y_{n,2}(t)$	Under attack output
z_f	Filtered $y_{n,2}(t)$
A_f	A stable matrix
$C_{n,1}$	Coefficient matrix related to $y_{n,1}(t)$
$C_{n,2}$	Coefficient matrix related to $y_{n,2}(t)$
$x(t)$	New states after filtering
A	System matric after filtering
B	Coefficient matrix for system input after filtering
B_{nld}	Coefficient matrix for deregulated bidding market and load variations after filtering
F_n	Load and bidding market variation
$E_{s,n}$	Coefficient matrix for the cyber-attack effect after filtering
$F_{s,n}$	False data cyber attack
y	System output after filtering
C	Output coefficient matrix after filtering
$w_m(t)$	Matched disturbances
$w_u(t)$	Unmatched disturbances
$e(t)$	Tracking error
$r(t)$	Desired reference signal
D	An open vicinity of the EP
$\hat{D}$	Subset of D
x_0	Initial condition
$t_1(x_0)$	Convergence time
ξ, k_1, k_2	A constant
ς	A small constant which does not affect to sign of the ξ
$s_e(t)$	Sliding surface
$V(t)$	Lyapunov function
k_p, k_i and k_d	Positive scalar values in PID sliding mode surface design
β	Decay rate of $s_e(t)$, ($\beta > 0$)
$u(t)_{eq}$	Equivalent control law
$u(t)_{sw}$	Switching controller
λ	A designed constant
$sgn(.)$	The sign function
Υ	A designed constant
$\bar{t}$	Time that the tracking errors reach the ε
$\hat{k}_s(t)$	Control gain
ε	Vicinity of the PID sliding surface
$\bar{t}$	Time that the tracking errors reach the vicinity of the PID sliding surface
$k_{s_a}(t)$	Adaptation law
$k_{s_{psb}}(t)$	positive-semi-definite barrier function
ℓ	A positive coefficient
σ	Convergence region
φ	A positive scalar,
k_s	An unknown positive factor

I. Introduction

With the advent of bidirectional communication infrastructure and digitalization features, power systems are transitioning from a vertical and monopolistic structure to a competitive one. Contrary to the vertical structure, independent system operators supervise bilateral contacts between power market participants in the deregulated market by considering total system efficiency and social welfare. In a deregulated power system, the exchanged energy between GENCOs and energy DISCOs depends on the energy prices [1]. Fluctuations in energy prices, which arise from bidding strategies implemented by GENCOs create a competitive environment in the energy exchange market. The quantity of power procured by i^{th} DISCO from j^{th} GENCO is affected by electricity price, affecting decision-making within the AGC framework and resulting in power flow and frequency oscillations accordingly [2].

The electricity market environment, especially the real-time bidding market, heavily depends on integrating ICT with the power system. ISOs manage real-time bidding markets in the energy sector, relying on SCADA systems. These ICT based systems play a vital role in monitoring and controlling energy processes and infrastructure in real-time, facilitating electricity transmission, grid operations, and market transactions. On the other hand, the integration of communication infrastructure, digitalization features, and Internet of Things technologies has rendered smart grids vulnerable to cyber-attacks [3, 4]. Attackers attempt to manipulate the measured data, transferred information, commands, and reference points by installing malware in intelligent electrical devices through physical or remote access or hijacking communications [5]. In general, several cybersecurity measures can be implemented, such as anti-malware, power system segmentation and firewall between segmentations, hardening access points, multi-step authentication, and security mechanism provided by IEC62351 standard series. However, some practical limitations in adapting these mechanisms and the evolving capabilities of cyber-attackers continue to render the smart grid vulnerable to these threats [6]. Attackers actively seek out system weaknesses to execute successful attacks.

In the real-time bidding market, the behavior of both GENCOs and DISCOs is unpredictable. This unpredictability and the inherent fluctuation of the bidding market create a highly uncertain environment, posing challenges for system operators to distinguish between false and accurate data. Furthermore, the power market requires new network paths and communications infrastructure. Therefore, these situations can be considered as a potential vulnerability within system operation and control [7, 8]. While specific attacks on the electricity market in real world may not be extensively documented, numerous real-world cyberattacks have targeted SCADA systems in the literature, including infamous instances like Stuxnet [9] and Black Energy [10] cyber-attacks.

The possible impact of false data injection cyber-attacks on AGC under deregulated power systems has been studied in [11]. As investigated in [7, 12], a cyber-attack that goes undetected by ISO can manipulate the power market integrity by injecting the false

data, resulting in a significant economic loss. In [13], the effect of the false data injection cyber-attack on economic costs in the Australian electricity market has been studied. As shown in [14], the impact of a false data injection attack on real time power market is more severe than false data injection attack on power demand. To defense against cyber-attack, in [15] cyber-vulnerability analysis for real-time power market operation has been proposed.

Coordination between various GENCOs and DISCOs simultaneously maintains grid frequency stability while considering market signals is performed by AGC [16]. Thus, it responds not only to changes in demand but also to price signals from real-time bidding markets. It faces challenges in a real time power market, including coordination among multiple GENCOs and DISCOs, ensuring technical participation of GENCOs, considering the dispatching limitations, managing congestion, and balancing economic considerations with grid reliability as well as data integrity due to the cyber-attack, especially the received signals from real time bidding market. Advanced secondary control strategies and improved communication protocols address these challenges. Secondary control systems act as a safety shield by cross-verifying and validating data from various sources before influencing AGC decisions, providing an added layer of protection. Considering this fact, to counteract cyber-attacks on the smart grid, various robust and efficient secondary controllers have been developed in SCADA system, such as active disturbance rejection control [17], resilient distributed coordination control [18], dynamic event-triggered output feedback control [19], model predictive control [20], SMC [21], H_∞ control [22, 23], fuzzy-logic control [24], and adaptive finite-time tracking control strategy [25]. The essential attributes expected from cyber defense controllers extend beyond cyber resiliency and encompass high precision, convergence to EPs within a finite time and swift response even in the face of matched and unmatched disturbances, uncertainties, and nonlinearities, which means that the system response returns to the permissible frequency range within a finite time after deviating due to unexpected faults, load changes, or cyber-attacks. Considering the eye-catching advantages of SMC with asymptotic stability, such as robustness against parametric uncertainties, delays, matched and unmatched internal and external disturbances [26], researchers have improved its performance by eliminating its limitations.

Several SMC techniques, including non-singular terminal SMC [27], second-order SMC [28], finite SMC [29], fractional-order SMC [30], and adaptive non-singular finite time SMC [26], have been proposed to enhance the system stability. Conventional SMC with linear sliding surfaces based on the design strategy for reaching and switching can exhibit different behaviors, particularly in terms of robustness features [31]. The primary obstacle encountered when applying SMC to address cyber-attacks is the occurrence of chattering phenomena. These phenomena manifest as high-frequency oscillations in the system's control law, which can impede the effective rejection of cyber-attacks and potentially lead to system instability [32]. To mitigate the chattering phenomenon, researchers have designed second-order sliding surface [33, 34]. Another issue with SMC is its property of asymptotic stability, which guarantees slow convergence to EPs over an infinite time horizon [35]. However, this characteristic poses a challenge when it comes to the practical application of SMC for online cyber-attack rejection. In real-time scenarios, where timely and efficient cyber-attack response is critical, the reliance on infinite-time slow convergence becomes impractical. Given the rapid dynamics observed in the smart grid performance, achieving convergence within a specified time frame becomes crucial, aligned with the concept of finite-time stability [26]. Therefore, fast convergence is essential to ensure effective control and response in real-time bidding markets in smart grids, especially in the presence of cyber-attacks. To enhances the convergence speed, researchers have proposed, the finite-time trajectory tracking approach [36].

Participation of GENCOs and DISCOs within the real-time electricity market, facilitated by the secondary hierarchical control layer under the described severe uncertainty conditions, introduces a new aspect to the real-time bidding market of the power system. Effectively addressing these challenges is vital to ensure the resilience and efficiency of the power system in adapting to fluctuating demand and evolving market conditions. To this end and considering the mentioned advantages and practical limitations of the SMC and discussed solutions for removing the limitations, this paper presents a novel SMC based strategy as a secure secondary hierarchical control layer to address the diverse challenges encountered by smart grids operating in a real-time bidding market, including cyber-attack rejection, robustness against parametric uncertainties, both matched and unmatched internal and external disturbances, and time delays. The proposed method introduces an innovative barrier-function adaptive finite-time trajectory tracking control approach that enables resilient operation and precise trajectory tracking within a finite time duration. This approach overcomes the limitations associated with conventional SMC, additionally, the application of an adaptive barrier function guides the output variable towards a predetermined vicinity of zero, irrespective of the upper bound of matched and unmatched internal and external disturbances, without negatively impacting the control gain for oversetting [37-39].

The proposed method, incorporating the mentioned features such as high accuracy, good transient performance, smooth control, and the ability to reject false data cyber-attacks in the presence of parametric uncertainties, matched and unmatched internal and external disturbances, and time delays, emerges as a practical controller for smart grid operations, providing a promising solution to enhance the performance and security in real-time bidding markets.

The main contributions of this paper are summarized as follows:

- Introducing a new aspect to the bidding market in the power system, as the participation of GENCOs and DISCOs in the real-time power market, subject to false data injection cyber-attacks and uncertainties.
- Developing a novel chattering-free method with trajectory tracking within a finite time, high convergence rate, and accuracy for cyber-attack defense in real time power system bidding market;
- Addressing the inherent limitations of the smart grid, including uncertainties, matched and unmatched internal and external disturbances, and time delays while concurrently rejecting false data cyber-attacks.

The rest of the parts of this paper are arranged as follows. The problem formulation for the smart grid resiliency in the bidding market is defined in Section II. Section III presents the proposed method for solving the formulated problem. Test results and discussion are demonstrated in Section IV. Finally, the work conclusions are described in Section V.

II. Problem Formulation

In the traditional power market, the contracts established between GENCOs, and DISCOs are typically regarded as fixed and not real-time. These contracts are predetermined and remain unchanged over a specific period, usually based on long-term agreements or predefined terms. Contrastingly, the deregulated market establishes a competitive environment where contracts can undergo changes in response to real-time information. In this setting, GENCOs actively participate in AGC, while DISCOs are granted the opportunity to enter into contracts with GENCOs in other control areas, adhering to the market rules. [1]. Fig. 1 shows a conceptual view of the new aspect to the real-time bidding market in the power system.

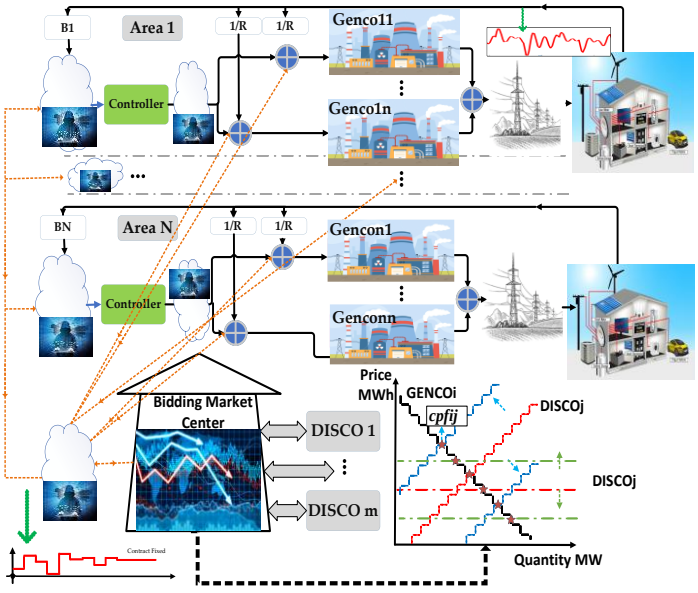

Fig. 1. A schematic diagram of the real-time power market.

The amount of the contract between GENCO i and DISCO j is specified by *cpfij*, where changing the amount of *cpfij* shows the contract changes between GENCO i and DISCO j. Multiple contracts can exist between GENCOs and DISCOs. These operations are executed under the direct observation of an independent system operator. All those contracts can be visualized in the DPM matrix. For example, a contract between six GENCOs and six DISCOs is shown as follows:

$$\text{DPM} = \begin{bmatrix} cpf_{11}cpf_{12}cpf_{13}cpf_{14}cpf_{15}cpf_{16} \\ cpf_{21}cpf_{22}cpf_{23}cpf_{24}cpf_{25}cpf_{26} \\ cpf_{31}cpf_{32}cpf_{33}cpf_{34}cpf_{35}cpf_{36} \\ cpf_{41}cpf_{42}cpf_{43}cpf_{44}cpf_{45}cpf_{46} \\ cpf_{51}cpf_{52}cpf_{53}cpf_{54}cpf_{55}cpf_{56} \\ cpf_{61}cpf_{62}cpf_{63}cpf_{64}cpf_{65}cpf_{66} \end{bmatrix} \quad (1)$$

The matrix rows are related to the GENCOs, and the matrix columns are related to the DISCOs. Each column of the matrix shows the contracts of one DISCO, and the sum of each column must be 'one' [16].

$$\sum_{i=1}^{n} cpf_{im} = 1 \quad (2)$$

where n is the numbers of GENCOs, and m indicates the m^{th} DISCOs. For example, $cpf_{61} = 0.2$ expresses that the DISCO 6 buys 0.2 PU needed power from GENCO 1. In (1), the diagonal elements demonstrate the local demand, and off-diagonal elements point out the contribution from other areas [16]. In the traditional power system, the ACE signal, which represents the sum of the input errors to the controller in each area, is defined as:

$$ACE_i = \Delta P_{tie,i} + \beta_{d,i}\,\Delta\omega_i \quad (3)$$

The frequency bias coefficient is defined as:

$$\beta_{d,i} = \frac{1}{R_{G,i}} + D_{p,i} \quad (4)$$

As mentioned earlier, in the deregulated power system, DISCOs in any control area are allowed to contract with each GENCOs in any control area. Therefore, the ACE signal in the deregulated environment differs from (3) and is modified as:

$$ACE_{d,i} = \Delta P_{tie,i} + \beta_{d,i}\Delta\omega_i - \left[\sum_{\substack{j=1 \\ j\neq i}}^{N}\left(\sum_{k=1}^{n} cpf_{kj}\right)\Delta P_{L,j} - \sum_{\substack{k=1 \\ j\neq i}}^{n}\left(\sum_{j=1}^{N} cpf_{jk}\right)\Delta P_{L,i}\right] \quad (5)$$

where N represents the number of control areas. Multiple GENCOs with different specifications participate in a deregulated environment. Some are responsible for AGC actions, and the participation rate differs for all participants. Considering their specifications, an *apf* is defined for each GENCO. The parameter *apf* denotes the contribution of each GENCO within a specific area to compensate for ACE signal in that area. The sum of participation rates in each control area equals one, as follows [1, 40].

$$\sum_{j=1}^{m} apf_j = 1 \quad (6)$$

In a deregulated power system, with the presence of multiple GENCOs in each control area, the governing differential equations are defined as [16]:

$$\Delta\dot{\omega}_i = \frac{1}{2H_i}\left(\sum_{k=1}^{n}\Delta P_{mech,k,i} - \Delta P_{tie,i} - load\ variation_i - D_{p,i}\Delta\omega_i\right) \quad (7)$$

$$\Delta P_{tie,i} = \frac{1}{S}\left(\sum_{\substack{j=1 \\ j\neq i}}^{N} T_{ij}\Delta\omega_i - \sum_{\substack{j=1 \\ j\neq i}}^{N} T_{ij}\Delta\omega_j\right) \quad (8)$$

$$\Delta\dot{P}_{tie,ij} = T_{ij}(\Delta\omega_i - \Delta\omega_j) \quad (9)$$

$$\Delta\dot{P}_{mech,k,i} = -\frac{1}{T_{t,k,i}}\Delta P_{mech,k,i} + \frac{1}{T_{t,k,i}}\Delta P_{valve,k,i} \quad (10)$$

The governor dead-band nonlinearity creates oscillations like a sine wave with approximately two-seconds natural periods. As discussed in [41], the Fourier series can be used to extract an exact nonlinear model for the governor as:

$$\Delta P_{valve} = \frac{0.8-\frac{0.2}{\pi}s}{1+sT_G}u(t) \quad (11)$$

where $u(t)$ indicates the governor's input. The control center receives the measured data and, after analysis, sends new references to the GENCOs for load following control accordingly. The process is time-consuming, and the time delay effect can be considered a delay in the system input. Considering the nonlinearity, time delay, and ACE participation factor the governing differential equation for governor can be expressed as

$$\Delta\dot{P}_{valve,k,i} = \frac{-0.8}{T_{G,k,i}}\left(\frac{1}{R_{G,k,i}}\Delta\omega_i + \Delta P_{valve,k,i} - apf_k \times u_i(t-\tau) - \sum_{\substack{j=1 \\ j\neq i}}^{m} cpf_{kj}\,\Delta P_{L,j}\right) + \frac{0.2}{\pi\times T_{G,k,i}} f_n(u(t-\tau), x(t)) \quad (12)$$

The new aspect of the real-time bidding market in the power system can be visualized by the appearance of the time variance nature of the cpf_{kj} in (12), as well as the differential equation governing the system. Consequently, following the contract changes due to the offered price by GENCO j in the bidding

market, the states of the system will also change. Therefore, until reaching a new agreement, the balance of the biddings between DISCO i and GENCO j will be lost, i.e., $\sum_{j=1}^{N} cpf_{ik} \neq 1$. As a result, the power system frequency will oscillate due to a lack of balance between generation and consumption. Adding to the complexity of the problem, the power fluctuations in the bidding market create a high potential environment for launching stealthy cyber-attacks. Considering the cyber-attack effects, the (5) and (12) change as (13) and (14), respectively.

$$\begin{aligned} ACE_{d,i} &= \Delta P_{tie,i} + \beta_{d,i}\Delta f_i \\ &\quad - \left[\sum_{\substack{j=1 \\ j\neq i}}^{N}\left(\sum_{k=1}^{n} cpf_{kj}\right)\Delta P_{L,j}\right. \\ &\quad \left. - \sum_{k=1}^{n}\left(\sum_{\substack{j=1 \\ j\neq i}}^{N} cpf_{jk}\right)\Delta P_{L,i}\right] + \boldsymbol{fdi_{o,i}} \end{aligned} \tag{13}$$

$$\begin{aligned} \Delta\dot{P}_{valve,k,i} &= \frac{-0.8}{T_{G,k,i}}\left(\frac{1}{R_{G,k,i}}\Delta\omega_i + \Delta P_{valve,k,i} - apf_k\right. \\ &\quad \left. \times u_i(t-\tau) - \sum_{\substack{j=1 \\ j\neq i}}^{N} cpf_{kj}\,\Delta P_{L,j}\right) \\ &\quad + \frac{0.2}{\pi \times T_{G,k,i}} f_n(u(t-\tau), x(t)) + \boldsymbol{fdi_{s,i}} \end{aligned} \tag{14}$$

States in the area i are:

$$X_i = [\Delta P_{tie,i}\ \Delta\omega_i\ \cup_{j=1}^{n}(\Delta P_{valve,j,i}, \Delta P_{mech,j,i})] \tag{15}$$

The states in the area i increase as the number of GENCOs increases. The state equation governing the dynamics of a smart grid in area i can be expressed as:

$$\begin{cases} \dot{x}_{n,i}(t) = A_{n,i}x_{n,i}(t) + B_{n,i}u_{n,i}(t-\tau) + \sum_{j=1}^{N} A_{n,ij}x_{n,j}(t) + \\ \qquad B_{lv}u_{lv}(t) + B_{mb}u_{mbs}(t) + B_{fdi,s}fdi_{s,i}(t) + \\ \qquad f_n(u_n(t-\tau), x(t))) \\ y_{n,i}(t) = C_{n,i}x_{n,i}(t) + D_{mb,i}u_{mbo,i}(t) + E_{fdi,o}fdi_{o,i}(t) \end{cases} \tag{16}$$

where in the real-world applications, frequency fluctuation and transferred power between controlling areas as well as the ACE signal are the system outputs, caused by bidding market dynamics, load variations, and the potential impact of cyber-attacks through false data injection.

A new aspect of the real-time bidding market multiarea power system under false data injection cyber-attack with integration the $\sum_{j=1}^{N} A_{n,s,ij}$ into $A_{n,i}$ can be expressed by the following the state-space representation:

$$\begin{cases} [\dot{x}_n(t)] = [A_n]_{n\times n}x(t) + [B_n]_{n\times nc}u(t-\tau) + [B_{lv}]_{n\times nlv}u_{lv}(t \\ \qquad +[B_{mb}]_{n\times nmbs}u_{mbs}(t) + \\ \qquad [B_{fdi,s}]_{n\times ns}fdi_s(t) + f_n(u(t-\tau), x_n(t)) \\ [y_n(t)]_{p\times 1} = [C_n]_{p\times n}x(t) + [D_{mb}]_{p\times nmbo}u_{mbo}(t) + \\ \qquad [E_{fdi,o}]_{p\times no}fdi_o(t) \end{cases} \tag{17}$$

It is worth to mention that, if each area has one controller nc will be equal with the number of areas. Since for each controlling area we consider a lumped load variation, therefore, nlv is equal with the number of the areas. Inspired by [42], it can displace the under-attack outputs to state equations as augmented states. For this purpose, a simple approach is employed to decompose the system output into two sub-outputs. One is the outputs without cyber-attacks and direct input from the bidding market, and the second one includes the outputs with cyber-attacks and direct input from the bidding market with the help of a simple orthogonal decomposition matrix (T_{or}). A stable filter is then designed to displace the under-attack outputs into the state equations. This method is easy and applicable compared to the complex decomposition method, which tries to decompose whole states and the system.

Assumption 1: rank ($E_{fdi,o}$)=rank (D_{mb})

In a multiarea power system, each controlling area has a central controller, which receives data from the many sensors to evaluate and send back the proper commands. It is worth mentioning that although the attack location is unknown in practice, the effect of a cyberattack can be seen in the transmitted signals, which are the central control input and output. T_{or} must be able to partition $E_{fdi,o}$ and D_{mb} as

$$\begin{aligned} T_{or} \times [E_{fdi,o}] &= \begin{bmatrix} 0 \\ E_{fdi,o,2} \end{bmatrix} \\ T_{or} \times [D_{mb}] &= \begin{bmatrix} 0 \\ D_{mb,2} \end{bmatrix} \end{aligned} \tag{18}$$

where $E_{fdi,o,2}\epsilon R^{no}$, and $D_{mb,2}\epsilon R^{no}$. Let multiply the T_{or} to the system output.

$$\begin{aligned} &T_{or} \times y_n(t) \\ &= \begin{cases} [y_{n,1}(t)]_{p-no\times 1} = [C_{n,1}]_{p-no\times n}x_n(t) \\ [y_{n,2}(t)]_{no\times 1} = [C_{n,2}]_{no\times n}x_n(t) + \\ \quad [D_{mb,2}]_{no\times nmbo}u_{mbo}(t) + [E_{fdi,o,2}]_{no\times no}fdi_o(t) \end{cases} \end{aligned} \tag{19}$$

A stable filter is designed to displace $y_{n,2}(t)$ into the state equation, as

$$\dot{z}_f(t) = A_f z_f(t) - A_f y_{n,2}(t) \tag{20}$$

where $z_f(t)\epsilon R^p$ is the filtered $y_{n,2}(t)$ and A_f is a stable matrix. With applying the filter, (17) changes as

$$\begin{cases} \underbrace{\begin{bmatrix} \dot{x}_s(t) \\ \dot{z}_f(t) \end{bmatrix}}_{\dot{x}(t)} = \underbrace{\begin{bmatrix} A_n & 0 \\ -A_f C_{n,2} & A_f \end{bmatrix}}_{A}\cdot\underbrace{\begin{bmatrix} x_n \\ z_f(t) \end{bmatrix}}_{x(t)} + \underbrace{\begin{bmatrix} B_n \\ 0 \end{bmatrix}}_{B}\cdot\underbrace{u_n(t-\tau)}_{u(t-\tau)} + \\ \qquad \underbrace{\begin{bmatrix} B_{lv} & B_{mb} & 0 \\ 0 & 0 & -A_f D_{mb,2} \end{bmatrix}}_{B_{nld}}\cdot\underbrace{\begin{bmatrix} u_{lv}(t) \\ B_{mb}(t) \\ u_{mbo}(t) \end{bmatrix}}_{F_n} + \\ \underbrace{\begin{bmatrix} B_{fdi,s} & 0 \\ 0 & -A_f E_{fdi,o,2} \end{bmatrix}}_{E_{s,n}}\cdot\underbrace{\begin{bmatrix} fdi_o(t) \\ fdi_l(t) \end{bmatrix}}_{F_{s,n}} + \underbrace{\begin{bmatrix} f_n(u_n(t-\tau), x(t)) \\ 0 \end{bmatrix}}_{f_n(x,t)} \\ \underbrace{\begin{bmatrix} y_{n,1}(t) \\ z_f(t) \end{bmatrix}}_{y} = \underbrace{\begin{bmatrix} C_{n,1} & 0 \\ 0 & I \end{bmatrix}}_{C}\cdot\begin{bmatrix} x_n(t) \\ z_f(t) \end{bmatrix} \end{cases} \tag{21}$$

With the new variables, the state-space model is formed as

$$\begin{cases} \dot{x}(t) = Ax(t) + Bu(t-\tau) + \underbrace{B_{nld}F_n}_{w_m(t)} + \\ \qquad \overbrace{E_{s,n}F_{s,n}(t)}^{w_u(t)} + f_n(x,t) \\ y(t) = Cx(t) \end{cases} \tag{22}$$

The behavior of the F_n is same as the matched disturbances while the cyber-attack effect can be modeled by unmatched disturbances.

This work aims for the smooth operation of the nonlinear delayed input system in (22), which simultaneously is under cyber-attack and parametric uncertainties and matched internal and external disturbances.

III. Proposed Method

To model a nonlinear delayed input smart power system within a bidding market, subject to cyber-attack, a stable filter was

designed as well as simplification of mathematical equations by substituting new variables, leading to the derivation of (20).To design the proposed barrier-function adaptive finite-time trajectory tracking control, considering a new representation of (20) as:

$$\dot{x}(t) = Ax(t) + B\big(u(t-\tau) + w_m(t)\big) + w_u(t) + f_n(x,t), \quad (23)$$

$$y(t) = Cx(t)$$

where $x(t) \in R^n$ denotes the system states, $y(t) \in R^p$ represents the output, $u(t) \in R^m$ signifies the controller input, $w_m(t)$ and $w_u(t)$ are the matched and unmatched perturbations, A, B, C show the system parameters, and R symbolizes a set of all real values. The control purpose is to determine a suitable mechanism to confirm that the system output tracks the desired reference signal $r(t)$ under perturbations. The tracking error signal is formed as

$$e(t) = y(t) - r(t) \quad (24)$$

This paper aims to present an adaptive barrier-function-based second order sliding mode control approach, specifically designed to mitigate false data injection cyber-attack challenges within the real-time bidding market of the power system modeled in (23). The design methodology comprises four primary steps:

- Finite time stabilization requirements
- Sliding surface design
- Proposed control strategy
- Adaptive barrier function law design

Our goal is to mitigate false data injection cyber-attack challenges within the real-time bidding market of the delayed uncertain power system. To this end, all the mentioned assumptions are precisely considered according to the governing conditions of the real-world AGC system and real-time bidding market in a deregulated environment. The ACE signal is consistently checked, and an alarm system is activated to promptly notify the operator in the event of any irrational conditions mentioned in [43]. On the other hand, changing rates of the output power of the generation units are limited by the power plants' technical limitations, such as turbine and generator constraints, heat and cooling systems limitations, transmission and grid interface, response time, etc.

Assumption 2: The disturbance $w_m(t)$ satisfies the matched condition.

Assumption 3: $w_m(t)$ and $w_u(t)$ are bounded disturbances.

A. Finite Time Stabilization Requirements

***Definition 1*:** Supposing a defined system by

$$\dot{x}(t) = f(x), \quad (25)$$

where $f(x): D \to R^n$ is a nonlinear time-invariant continuous vector function defined on an open vicinity D of the EP. The EP shows the power system under normal and stable conditions, which reflects frequency stability. The EP will become locally stable within a finite period if the next-mentioned requirements are met:

- Asymptotically stable in the subset $\widehat{D} \subseteq D$.
- Convergent in $\widehat{D}$ in the finite-time. This means that there exists a convergence time $t_1(x_0)$ such that $x(t, x_0) \to 0$ as $t \to t_1(x_0)$ and remains zero thereafter. Besides, if $\widehat{D} = R^n$, the EP will be globally stable within a finite period.

Definition 2: Considering the following affine nonlinear time-invariant system:

$$\dot{x}(t) = f(x) + g(x)u(t-\tau), \quad (26)$$

where $x(t) \in R^n$ is the state variable, $u(t-\tau) \in R^m$ is the control input, $f(0) = 0$ and $g(x) \neq 0$. The $u(t-\tau) = \Pi(x, t-\tau)$ is named as a finite-time stabilizing control law if the EPs of the system (26) become stable in a finite-time.

Assumption 4: For a constant $\xi (\xi = k_1 + \varsigma$ for $u(t) \geq 0$, $k_2 + \varsigma$ for $u(t) \leq 0)$, the inequality $u(t-\tau) \leq \xi u(t)$ is satisfied [44]. where, $k_1 > 0$, $k_2 < 0$ and ς is a small constant which does not affect to sign of the ξ.

B. Sliding Surface Design

Definition 3: The sliding surface $s_e(t)$ is from order r if:

$$s_e(t) = \dot{s}_e(t) = \ddot{s}_e(t) = \cdots = s_e(t)^{(r-1)} = 0 \quad (27)$$

Lemma 1: Considering the candidate positive-definite Lyapunov function $V(t)$ with

$$\dot{V}(t) \leq -\alpha V(t) - \beta V(t)^{\eta} \quad (28)$$

where $t \geq t_0 (initial\ time), V(t_0) \geq 0, \alpha > 0, \beta > 0$, and η as a fraction of two odd positive integers $(1 > \eta > 0)$. The Lyapunov function $V(t)$ reaches the origin in the finite time t_s:

$$t_s \geq t_0 + \frac{1}{\alpha(1-\eta)} ln\left(\frac{\alpha V(t_0)^{1-\eta} + \beta}{\beta}\right) \quad (29)$$

The PID sliding mode surface is defined as

$$s_e(t) = k_p e(t) + k_i \int_0^t e(\tau) d\tau + k_d \dot{e}(t) \quad (30)$$

If the $e(0) = 0$ (initial error), then the tracking problem is supposed as the error remains on the sliding surface $s_e(t) = 0$ for all $t \geq 0$. If the system states trajectory reaches the sliding surface $s_e(t) = 0$, it stays on it until it goes into the origin. $e(t) = 0$ and $\dot{e}(t) = 0$. This paper uses the PID sliding surface to design a second order sliding mode controller. In a second order sliding mode, the purpose of the control law is to lead the $s_e(t)$ and $\dot{s_e}(t)$ to the equilibrium as $s_e(t) =, \dot{s_e}(t) = 0$. This surface is defined as

$$\dot{s_e}(t) + \beta s_e(t) = k_p e(t) + k_i \int_0^t e(\tau) d\tau + k_d \dot{e}(t) \quad (31)$$

The second time-derivative for $s_e(t)$ is obtained from (31) as

$$\ddot{s_e}(t) + \beta \dot{s_e}(t) = k_p \dot{e}(t) + k_i e(t) + k_d \ddot{e}(t) \quad (32)$$

The error trajectory will remain on the sliding surface $s_e(t)$ if $\dot{s_e}(t) = \ddot{s_e}(t) = 0$. Then, the characteristic polynomial is obtained as

$$\ddot{e}(t) + \frac{k_p}{k_d} \dot{e}(t) + \frac{k_i}{k_d} e(t) = 0 \quad (33)$$

C. Proposed Control Strategy

If the k_p, k_i and k_d are designed correctly, the roots of the characteristic polynomial in (33) will lie on the open left half of the complex plane as it will be strictly Hurwitz. In this condition, the tracking error $e(t)$ will exponentially converge to the origin. Considering assumption 4**,** the first and second-order time-derivative of the $e(t)$ are obtained from (23) and (24) as

$$\dot{e}(t) = C\big(Ax(t) + \xi Bu(t)\big) + M(t) - \dot{r}(t) \quad (34)$$

$$\ddot{e}(t) = CA\big(Ax(t) + \xi Bu(t)\big) + \xi CB\dot{u}(t) + N(t) - \ddot{r}(t) \quad (35)$$

where $N(t) = C(A(Bw_m(t) + w_u(t)) + B\dot{w}_m(t) + \dot{w}_u(t))$ and $M(t) = Cw_u(t) + CBw_m(t)$. Substituting (34) and (35) into (32) gives

$$\ddot{s_e}(t) + \beta \dot{s_e}(t) = k_p C\big(Ax(t) + \xi Bu(t)\big) + k_p M(t) - k_p \dot{r}(t) + k_i e(t) + k_d CA\big(Ax(t) + \xi Bu(t)\big) + \xi k_d CB\dot{u}(t) + k_d N(t) - k_d \ddot{r}(t) \quad (36)$$

The equivalent control law can be obtained if

- $\ddot{s_e}(t) = 0$
- $M(t) = 0$ and $N(t) = 0$.

$$\dot{u}(t)_{eq} = -(\xi k_d CB)^{-1}\big[\big(k_p C + k_d CA\big)\big(Ax(t) + \xi Bu(t)_{eq}\big) - k_p \dot{r}(t) + k_i e(t) - k_d \ddot{r}(t) - \beta \dot{s_e}(t)\big] \quad (37)$$

The switching controller is designed as

$$\dot{u}_{sw}(t) = -(\xi k_d CB)^{-1}\big[\big(k_p C + k_d CA\big)\xi B u_{sw}(t) + k_d \lambda |s_e(t)| sgn(\dot{s_e}(t)) + k_d k_s\, sgn(\dot{s_e}(t))\big] \quad (38)$$

where $\lambda > 1/k_d$ and $k_s > N_{max} + k_p M_{max}/k_d$ with $M_{max} = max|M(t)|$ and $N_{max} = max|N(t)|$. If the control law as

$$\dot{u}(t) = \dot{u}(t)_{eq} + \dot{u}(t)_{sw} \quad (39)$$

Substituting (37) and (38) into (36) finds

$$\ddot{s_e}(t) = k_p M(t) + k_d N(t) + \big(k_d CA + k_p C\big)\xi B u(t)_{sw} + \xi k_d CB \dot{u}(t)_{sw} = k_d N(t) + k_p M(t) - k_d \lambda |s_e(t)| sgn(\dot{s_e}(t)) - k_d k_s\, sgn(\dot{s_e}(t)) \quad (40)$$

The purpose of the presented approach is to employ the discontinuous term to operate on the $\dot{u}(t)$ such that the obtained controller becomes smooth, continuous, and chattering-free after integration.

Theorem 1: Considering the perturbed dynamic system in (23) and the PID sliding surface in (30), if the controller signal is designed as (39), then the error trajectories are started from all initial conditions and reach the PID sliding surface and stay on it thereafter.

Proof: Considering the positive-definite Lyapunov function $V(s_e(t), \dot{s_e}(t)) = 0.5(s_e(t)^2 + \dot{s_e}(t)^2)$, where using (31), one obtains

$$\dot{V}\big(s_e(t), \dot{s_e}(t)\big) = s_e(t)\dot{s_e}(t) + \dot{s_e}(t)\ddot{s_e}(t) = s_e(t)\dot{s_e}(t) + \dot{s_e}(t)(k_d N(t) + k_p M(t) - k_d \lambda |s_e(t)| sgn(\dot{s_e}(t)) - k_d k_s\, sgn(\dot{s_e}(t))) \quad (41)$$

where

$$\dot{V}(s_e(t), \dot{s_e}(t)) \le s_e(t)\dot{s_e}(t) + k_d N(t)\dot{s_e}(t) + k_p M(t)\dot{s_e}(t) - k_d \lambda |s_e(t)||\dot{s_e}(t)| - k_d k_s |\dot{s_e}(t)| \le -(k_d\lambda - 1)|\dot{s_e}(t)||s_e(t)| - \big(k_d k_s - k_d N_{max} - k_p M_{max}\big)|\dot{s_e}(t)| \le -2^{\frac{1}{2}}(k_d\lambda - 1)|\dot{s_e}(t)|\frac{|s_e(t)|}{2^{\frac{1}{2}}} - 2^{\frac{1}{2}}(k_d k_s - k_d N_{max} - k_p M_{max})\frac{|\dot{s_e}(t)|}{2^{1/2}} \le -2^{1/2}\, min\big\{(k_d\lambda - 1)|\dot{s_e}(t)|, k_d k_s - k_d N_{max} - k_p M_{max}\big\}\Big(\frac{|s_e(t)|}{2^{1/2}} + \frac{|\dot{s_e}(t)|}{2^{1/2}}\Big) \le -\Upsilon V(s_e(t), \dot{s_e}(t))^{1/2} \quad (42)$$

where $\Upsilon = 2^{1/2}\, min\big\{(k_d\lambda - 1)|\dot{s_e}(t)|, k_d k_s - k_d N_{max} - k_p M_{max}\big\}$.

It means from (41) that the time-derivative of the Lyapunov function is negative-definite, which indicates that $s_e(t)$ and $\dot{s_e}(t)$ tend to zero in the finite period of time. Hence, the tracking error signals in (34) are convergent to the sliding surface and stay on it thereafter. According to Theorem 1, using the discontinuous controller $\dot{u}(t)$ in (39), the PID-type sliding surface $s_e(t)$ and its time-derivative $(\dot{s_e}(t))$ are converged to zero in the finite period. Consequently, the control input $u(t)$ is a continuous function and overcomes chattering phenomenon. In practice, the upper bounds of the perturbation terms are considered unknown, making it challenging to determine the values of N_{max} and M_{max}. In what follows, in order to determine the unknown upper bounds of perturbations, an adaptive controller is designed, and a barrier function-based adaptive control technique is presented. With the adaptive barrier function, the control input is defined as

$$\dot{u}(t) = -(\xi k_d CB)^{-1}\big[\big(k_p C + k_d CA\big)\big(Ax(t) + \xi Bu(t)_{eq}\big) - k_p \dot{r}(t) + k_i e(t) - k_d \ddot{r}(t) - \beta \dot{s_e}(t) + \big(k_p C + k_d CA\big)\xi B u_{sw}(t) + (k_d\lambda |s_e(t)| + k_d \hat{k}_s(t))\, sgn(\dot{s_e}(t))\big] \quad (43)$$

with

$$\hat{k}_s(t) = \begin{cases} k_{s_a}(t), & \text{if} \quad 0 < t \le \bar{t} \\ k_{s_{psb}}(t), & \text{if} \quad t > \bar{t} \end{cases} \quad (44)$$

where $\bar{t}$ is the time that the tracking errors reach the vicinity ε of the PID sliding surface in (30).

D. Adaptive Barrier Function Design

The adaptation law $k_{s_a}(t)$ and the positive-semi-definite barrier function $k_{s_{psb}}(t)$ are suggested by

$$\dot{k}_{s_a}(t) = \ell |\dot{s_e}(t)| \quad (45)$$

$$k_{s_{psb}}(t) = \frac{|\dot{s_e}(t)|}{\varepsilon - |\dot{s_e}(t)|} \quad (46)$$

where ε and ℓ are the positive coefficients. Based on the adaptation law (45), the control gain $\hat{k}_s(t)$ is adjusted to increase until the tracking trajectories tend to vicinity ε of the PID sliding surface $s_e(t)$ and its time-derivative $\dot{s_e}(t)$ at time $\bar{t}$. For $\bar{t} > 0$, the controller gain $\hat{k}_s(t)$ switches to the positive-semi-definite barrier function $k_{s_{psb}}(t)$ which can diminish the convergence area and limit the tracking error states in that area. The stability of the perturbed system in (23) is considered in the subsequent conditions:

Condition (I): $\mathbf{0 < t \le \bar{t}}$

***Theorem 2*:** Referring to the perturbed system in (23) and the PID sliding surface in (30), for the times $0 < t \le \bar{t}$, the control input is shown as

$$\dot{u}(t) = -(\xi k_d CB)^{-1}\big[\big(k_p C + k_d CA\big)\big(Ax(t) + \xi Bu(t)_{eq}\big) - k_p \dot{r}(t) + k_i e(t) - k_d \ddot{r}(t) - \beta \dot{s_e}(t) + \big(k_p C + k_d CA\big)\xi B u_{sw}(t) + (k_d\lambda |s_e(t)| + k_d k_{s_a}(t))\, sgn(\dot{s_e}(t))\big] \quad (47)$$

with $\ell\varphi^{-1} < k_d$, the error trajectories approach the vicinity ε of the PID sliding surface in (30) in the finite time.

***Proof*:** The provided proof stability shows the stability of the designed control law. Due to a limited space, please refer to Appendix A for the details.

Condition (II): $\mathbf{t > \bar{t}}$

Theorem 3: Considering the uncertain system in (23) and the PID sliding surface in (30), for the times $t > \bar{t}$, if the adaptive control law is formulated as follows:

$$\dot{u}(t) = -(\xi k_d CB)^{-1}\Big[\big(k_p C + k_d CA\big)\big(Ax(t) + \xi Bu(t)_{eq}\big) - k_p \dot{r}(t) + k_i e(t) - k_d \ddot{r}(t) - \beta \dot{s_e}(t) + \big(k_p C + k_d CA\big)\xi B u_{sw}(t) + k_d\lambda |s_e(t)| sgn(\dot{s_e}(t)) + k_d k_{s_{psb}}(t)\, sgn(\dot{s_e}(t))\Big] \quad (48)$$

Then the states of the system reach the convergence region $|\sigma(t)| \le \varepsilon$ in the finite period.

Proof: To ensure the performance of the developed method, proof stability has been provided. Due to a limited space, please refer to Appendix A for the details.

The computational procedure of the suggested control strategy is depicted in Fig. 2. It comprises three sections, including:

- Defining the canonical form of the dynamic system.
- Designing the suggested method.
- Testing the developed method.

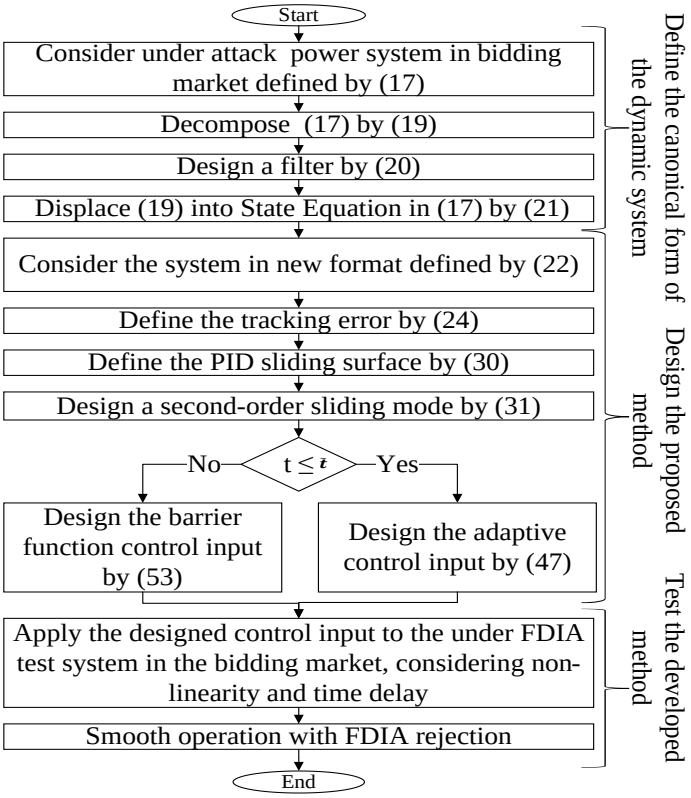

Fig. 2. Computational procedure of the proposed method.

IV. Test Results and Discussion

To ensure and demonstrate the performance of the proposed method, an IEEE 39-bus test system is selected and used for the study. Fig. 3 shows the one-line diagram of the test system. The understudy power system is subdivided into three areas. It is assumed that G1 and G3 in area 1, G4 and G7 in area 2, and G9 and G10 in area 3 are liable units for providing spinning reserves. The simulations are carried out to consider communication time delay and governor dead-bound nonlinearity in the real time bidding market, where the contract between DISCOs and GENCOs is changing until reaching the final agreement. The changes in contracts between GENCO '*i*' and DISCO '*j*' in the power bidding market are depicted in Fig. 4. The parameters of the studied system are listed in Table I [45]. In Fig. 4, the step change line labeled 1 represents the offered price by GENCO *i*, while lines labeled 2 to 4 illustrate the real-time bidding behavior of DISCO *j* in the market. The intersection of lines 1 with 2 to 4 signifies the contract between GENCO *i* and DISCO *j*. This visual representation reveals that when the price of electric power is high, DISCO *j* tends to purchase a lower amount of electricity (*cpfij*-High). Conversely, when the price is low, DISCO *j* tends to purchase a higher amount of electricity (*cpfij*-Low). The step changes in the contract have been accounted for considering the discrete nature of the energy prices. The horizontal lines 4 to 6 show the behavior of the DISCO *j* in bidding market, indicating that it has fixed contract with GENCO *i*.

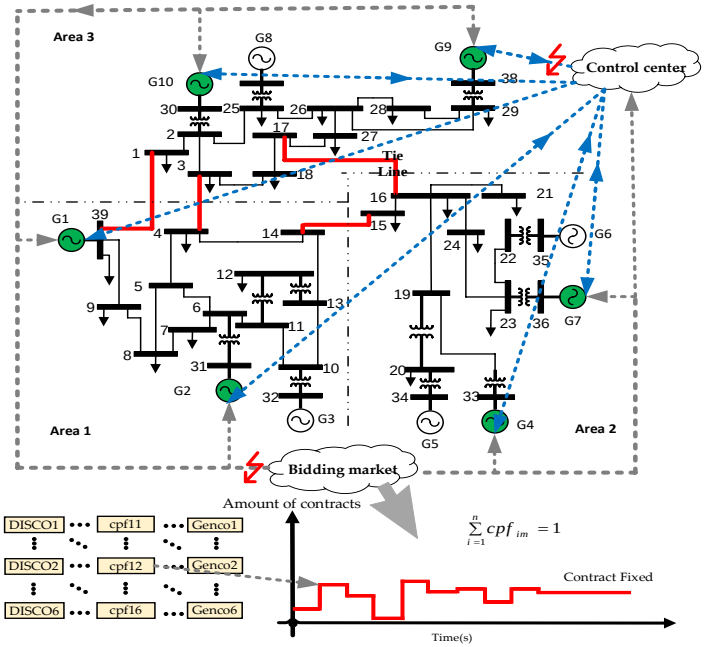

Fig. 3. IEEE 39-bus test system.

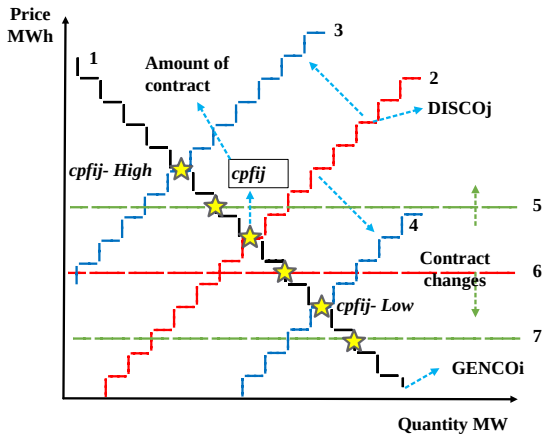

Fig. 4. Contract changes in the power bidding market.

TABLE I
PARAMETERS USED IN THE STUDY
(a) IEEE 39-bus TEST SYSTEM

GENCO	H	D	Governor time constant	Turbine time constant	Regulation parameter
1	70.0	1	0.08	0.04	0.23
2	30.3	1	0.08	0.04	0.12
3	35.8	1	0.08	0.04	0.15
4	28.6	1	0.08	0.04	0.14
5	56.0	1	0.08	0.04	0.12
6	34.8	1	0.08	0.04	0.14
7	26.4	1	0.08	0.04	0.14
8	24.3	1	0.08	0.04	0.13
9	34.5	1	0.08	0.04	0.17
10	20.0	1	0.08	0.04	0.06

(b) THE PROPOSED METHOD

k_p	k_i	k_d	k_s	β	ε	ℓ
2.4	0.1	3	1	1	0.01	0.65

As mentioned above, the fluctuation due to the changing power flow following contract changes in the bidding market creates a high potential environment for an attacker to launch a successful stealthy attack. The proposed method doesn't need cyber-attack detection for rejection, as proven the control laws guarantee to lead the system states toward the defined nonlinear sliding surface and keep them there in a finite time. In the analysis, a random

variable scaling attack is used to simulate the FDIA as shown as follows:

$$y(t) = \begin{cases} y(t) & Under\ Normal\ Conditon \\ (1 + \zeta(t))y(t) & Under\ Attack\ Condition \end{cases} \quad (49)$$

where $\zeta(t) \epsilon\ [-0.5\ 0.5]$ is a random variable function. It is simulated with white noise and shows the change in the power consumption until 0.5 pu, which is a realistic attack among the FDIAs. The 10% variation in the system parameters is assumed to evaluate the robustness of the developed method. As mentioned, FDIA has been simulated to occur in the online contract changing time.

To simulate the real time bidding power market effect, the DPM matrix elements (cpf_{ij}) with the mentioned condition in (2),$\sum_{i=1}^{n} cpf_{im} = 1$ are considered as step randomly functions, because the nature of the contract is step-change. For example, the contract simulation between GENCO 1 and DISCO 1 is depicted in Fig. 5. Considering the nature of randomly step functions of the bidding market, the total effects of the bidding market are shown in Fig. 6, where curves 1 to 9 show the input from bidding markets. Curves 1 to 6 are directly sent to the generation units, curves 7 to 8 are mapped into the ACE signal and are sent to the controller, and are defined as:

Curve1: $\sum_{i=1}^{6} cpf_{1i}$
Curve2: $\sum_{i=1}^{6} cpf_{2i}$
Curve3: $\sum_{i=1}^{6} cpf_{3i}$
Curve4: $\sum_{i=1}^{6} cpf_{4i}$
Curve5: $\sum_{i=1}^{6} cpf_{5i}$
Curve6: $\sum_{i=1}^{6} cpf_{6i}$
Curve7: Sum ($\sum_{i=3}^{6} cpf_{1i}$, $\sum_{i=3}^{6} cpf_{2i}$, $\sum_{i=1}^{2} cpf_{3i}$, $\sum_{i=1}^{2} cpf_{4i}$, $\sum_{i=1}^{2} cpf_{5i}$, $\sum_{i=1}^{2} cpf_{6i}$)
Curve8: Sum ($\sum_{\substack{i=1 \\ \neq 3,4}}^{6} cpf_{3i}$, $\sum_{\substack{i=1 \\ \neq 3,4}}^{6} cpf_{4i}$, $\sum_{i=3}^{4} cpf_{1i}$, $\sum_{i=3}^{4} cpf_{2i}$, $\sum_{i=3}^{4} cpf_{5i}$, $\sum_{i=3}^{4} cpf_{6i}$)
Curve9: Sum ($\sum_{i=1}^{4} cpf_{6i}$, $\sum_{i=1}^{4} cpf_{5i}$, $\sum_{i=5}^{6} cpf_{1i}$, $\sum_{i=5}^{6} cpf_{2i}$, $\sum_{i=5}^{6} cpf_{3i}$, $\sum_{i=5}^{6} cpf_{4i}$)

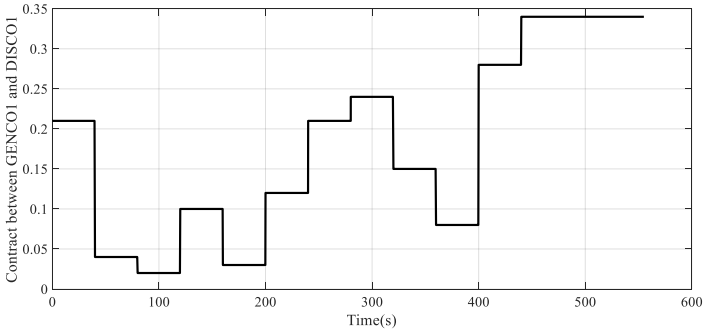

Fig. 5. The contract between GENCO 1 and DISCO 1.

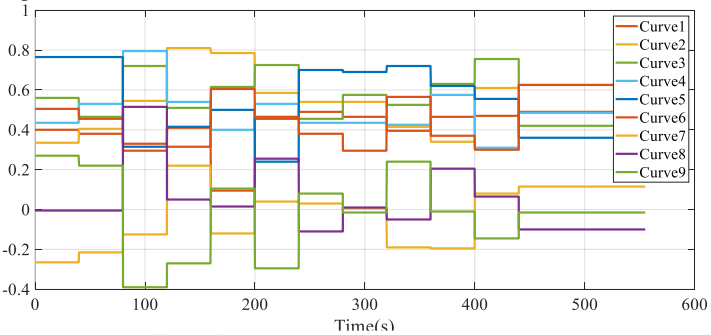

Fig. 6. The total effects of the bidding market.

The time trajectories of the power system frequency are shown in Fig. 7. According to Fig. 7, simultaneously changing contracts in the bidding power market and FDIA lead to frequency fluctuations. Test results illustrate that the developed method with the proper control signal removes the cyber-attack and frequency fluctuations within a short settling time. The time histories of the control inputs for settling the frequency fluctuations are given in Fig. 8. The effective performance of the proposed method in leading the state of the system toward the sliding surface and convergence can be seen in the time responses of the sliding surface as Fig. 9. To compare the performance of the developed method, an active disturbance rejection controller (ADRC) with performance in rejecting faults in uncertain environments proven in [42, 46] is used. Fig. 10 shows a comparison between the proposed method and an active disturbance rejection controller in regulating the power system frequency in the discussed power bidding market and FDICA conditions.

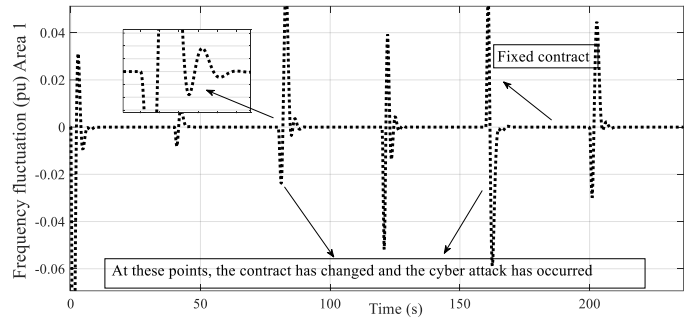

(a) Area 1

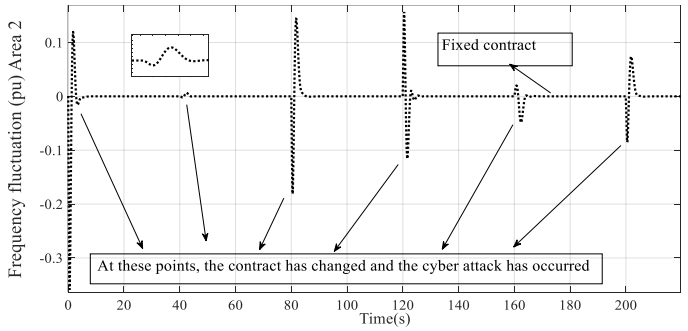

(b) Area 2

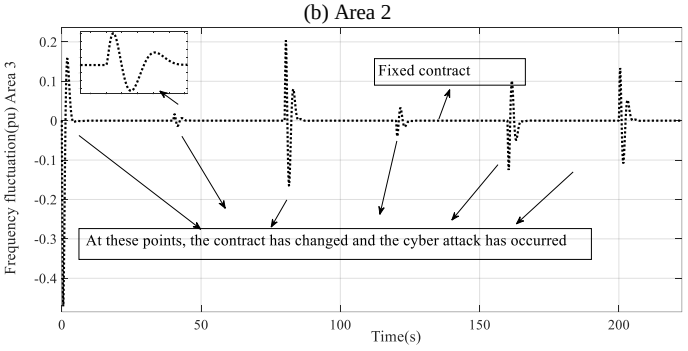

(c) Area 3

Fig. 7. Time trajectories of frequency fluctuations in different areas.

As shown in (5) and (12), in the power bidding market, contract changes directly affect central controllers and the governor of GENCOs. At the same time, FDIA affects controller inputs and outputs, as seen in (13). Therefore, the controllers fail to differentiate between this condition with the faulty condition and load variations, which leads to the issuance of new inaccurate reference points. As a result of the incorrect reference points, the output power of the GENCOs is regulated incorrectly, leading to the frequency of the power system going outside its limits. On the

other hand, the designed second order PID sliding surface in the proposed method creates strong robustness against both matched and unmatched conditions where false data cyber-attack and load variations as well as system uncertainties are considered. In addition, the finite time error trajectory tracking feature with the designed adaptive barrier function helps to diminish the convergence area, limit the tracking error states in that area, and guarantee convergence at a finite time, which results in fast and exact fluctuations tracking. Therefore, the mentioned features of the proposed method lead to sending the correct reference points simultaneously with cyber-attack rejection, resulting in frequency stability. Table II presents the main features of proposed method in comparison to conventional methods.

TABLE II
FEATURE COMPARISONS

Features / Methods	High convergence speed	Chatter free	Ability in fault rejection	Ability to distinguish between faults and FDIA.
Conventional controllers (PI, PID)	×	—	×	×
ADRC	×	—	✓	×
Conventional SMC	×	×	✓	×
Proposed method	✓	✓	✓	✓

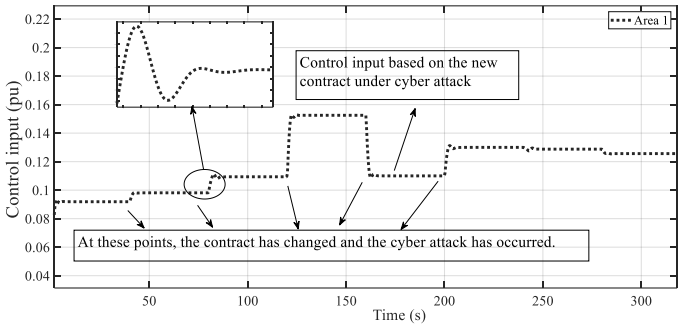

(a) Area 1

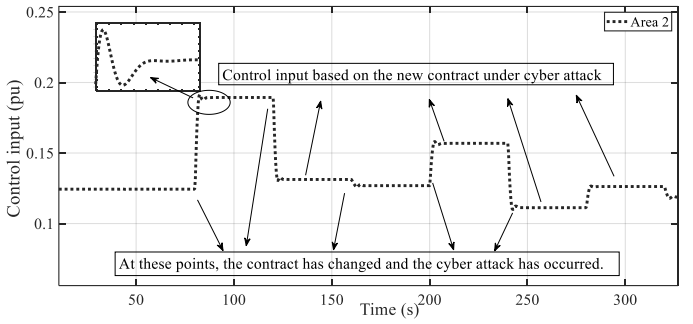

(b) Area 2

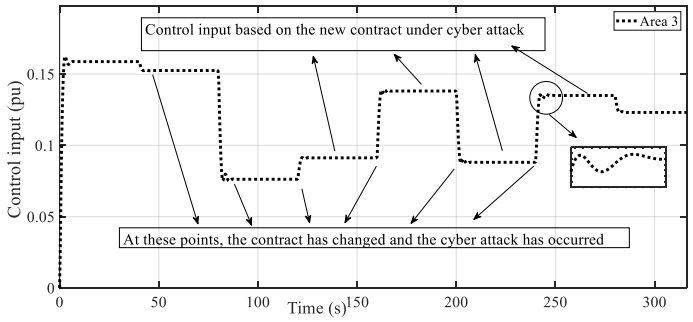

(c) Area 3

Fig. 8. Time histories of control input $u(t)$ in different areas.

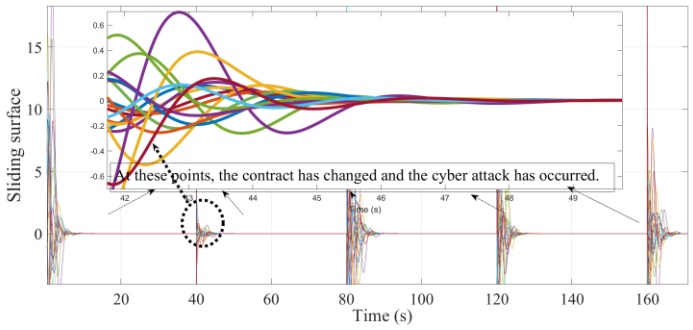

Fig. 9. Time responses of sliding surface convergence $s_e(t)$.

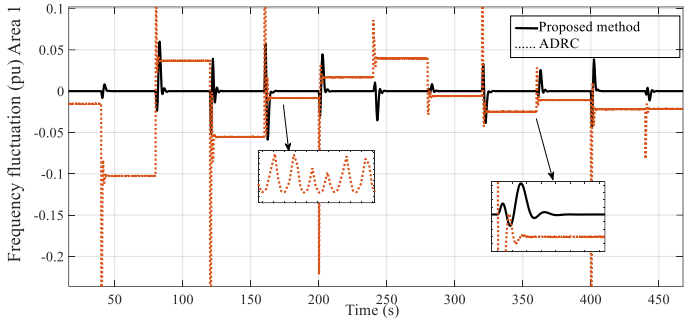

(a) Area 1

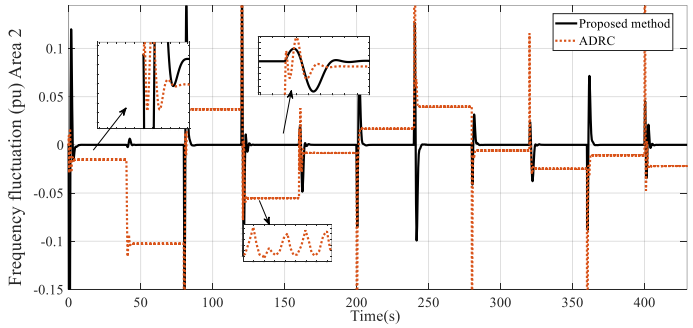

(b) Area 2

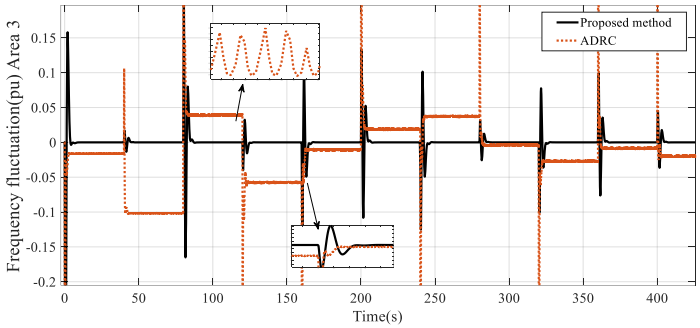

(c) Area 3

Fig. 10. A comparison of the frequency regulations in different areas.

When comparing the proposed method to ADRC, a notable advantage emerges in how they handle various operational scenarios. ADRC is unable to differentiate between different conditions such as faults, load fluctuations, and FDIC, leading to the generation of inaccurate reference points. This inaccuracy, in turn, causes errors in regulating the output power of the GENCOs, ultimately pushing the power system frequency beyond its intended operational range. In contrast, the proposed method takes a different approach by employing a stable filter that displaces outputs under attack to augmented system states. It then integrates a second-order PID sliding surface, showcasing impressive resilience across a range of scenarios. This includes effectively managing expected factors like load variations and unexpected ones such as false data cyber-attacks and system uncertainties. Moreover, the proposed method incorporates a finite-time error

trajectory tracking mechanism supported by the adaptive barrier function. This combination reduces the convergence area and confines tracking errors within this defined space to ensure a swift and accurate response to fluctuations. These distinctive attributes of the proposed method play a crucial role in ensuring the transmission of precise reference points while actively repelling cyber-attacks. Consequently, the system frequency stability can be effectively enhanced. Fig. 10 shows a comparison of the frequency regulations by the proposed method to those obtained by ARDC in the face of cyber threats.

The experimental test was performed to validate the effectiveness of the proposed control strategy in practical scenarios and prove the theoretical claims. The Speedgoat Real-Time Target Machine, along with Simulink real-time, provides a combined solution suitable for exploring and teaching design principles in various fields like mechatronics, motion control, power electronics, and signal processing. The Real-Time Target Machine acts as a robust platform for real-time simulation and testing. It comes with essential cables, terminal boards, and adapters to ensure smooth connectivity between the target machine's input/output (I/O) and the hardware being tested [47]. The Speedgoat real-time system consists of two main components: (1) a high-performance real-time target machine featuring an Intel 4.2 GHz i7 multi-core CPU, and (2) an IO306-Performance Simulink-programmable FPGA I/O module. The IO306 incorporates a Xilinx Kintex-7 FPGA with 64 x 3.3V TTL I/O lines and a Xilinx Spartan 6 FPGA with 24k logic cells. Simulink models can be automatically converted into code for either the CPU or FPGA using Simulink Real-Time or HDL Coder, respectively. Additionally, the Simscape Electrical model can be transformed into VHDL code using HDL Coder from MathWorks [48]. The real time experimental setup for testing the proposed method has been shown in Fig. 11. Fig. 12 presents the results of experimental tests conducted on the proposed method for real-time power system frequency regulation as well as convergence to sliding surface within a dynamic power market environment, even when subjected to cyber-attacks. The results highlight the system performance in terms of resilience and effectiveness in maintaining stable frequency levels amidst adversarial conditions.

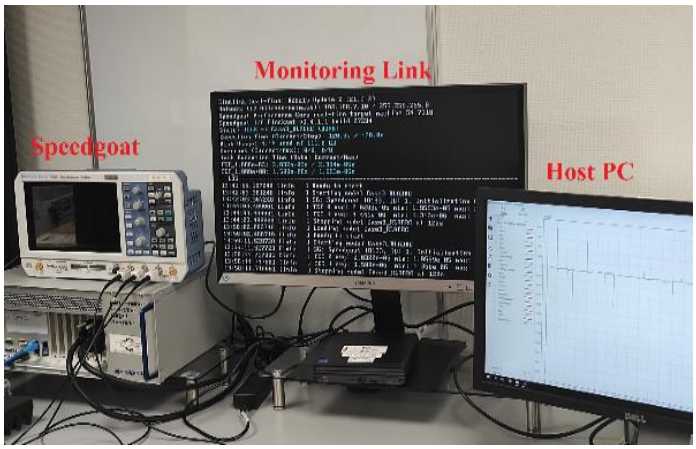

Fig. 11. Real-time experimental setup.

From the perspective of real-world implications, including implementation challenges and costs, the proposed barrier-function adaptive finite-time trajectory tracking control method is meticulously designed with real-world implementation in mind to ensure practical relevance and alignment with the complexities of operational environments. The assumptions taken in the design process are based on the real world, and the main strategy of the proposed method is based on the sliding mode controller, which is widely used in industry. Recognizing the role of the proposed method as a secure secondary controller within SCADA systems underscores its practical viability and the potential for market-driven incentives in securing critical systems against evolving cyber threats. Given the ongoing integration of information and communications technology and the transition toward autonomous operation in power systems to ensure system resilience with cyber-attack mitigation strategies has become the top priority. Considering this emphasis on system resilience, the implementation challenges, and costs, when compared to traditional methods, can be reasonably justified.

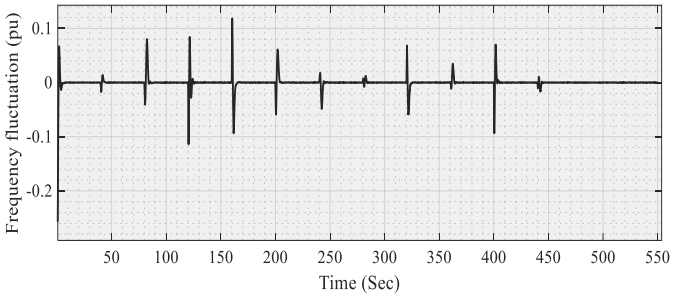

(a) Area 1

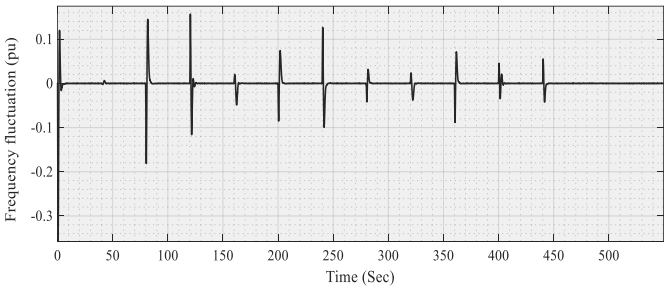

(b) Area 2

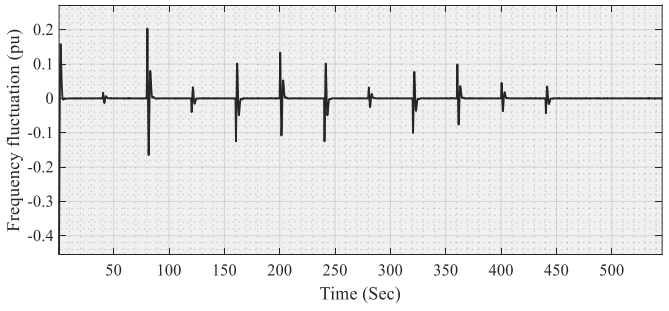

(c) Area 3

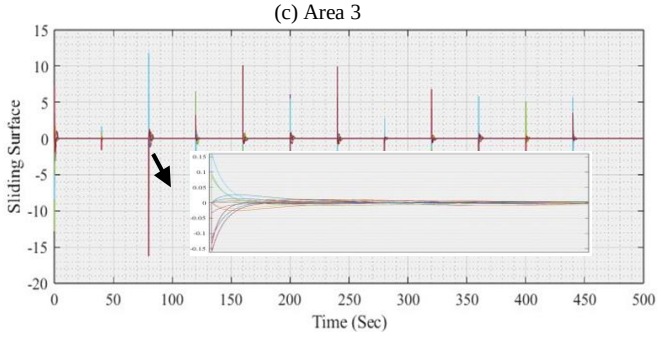

(d) Sliding surface convergence

Fig. 12. Experimental results of an IEEE 39-bus test system using the proposed method.

To demonstrate the scalability of the proposed method, different grid sizes and configurations are also selected and used to assess

its performance. Due to limited space, the results of an IEEE 118-bus test system [49] are presented. The test system comprises 54 synchronous machines, consisting of 19 generators, 20 capacitors, and 15 motors. The test system is divided into three control areas. Area 1 includes five synchronous generators, G10, G12, G25, G26, G31, Area 2 includes nine synchronous generators, G46, G49, G54, G59, G61, G66, G65, G69, G80, Area 3 includes five synchronous generators, G87, G89, G100, G103, G111. It is assumed that generators G10, G25, and G31 from area 1, G46, G59, G66, and G80 from are 2, and G87, G100, and G111 participate in the power market. Consider six DISCOs DPM matrix is designed as:

$$\text{DPM} = \begin{bmatrix} cpf_{11} & cpf_{12} & cpf_{13} & cpf_{14} & cpf_{15} & cpf_{16} \\ cpf_{21} & cpf_{22} & cpf_{23} & cpf_{24} & cpf_{25} & cpf_{26} \\ cpf_{31} & cpf_{32} & cpf_{33} & cpf_{34} & cpf_{35} & cpf_{36} \\ cpf_{41} & cpf_{42} & cpf_{43} & cpf_{44} & cpf_{45} & cpf_{46} \\ cpf_{51} & cpf_{52} & cpf_{53} & cpf_{54} & cpf_{55} & cpf_{56} \\ cpf_{61} & cpf_{62} & cpf_{63} & cpf_{64} & cpf_{65} & cpf_{66} \\ cpf_{71} & cpf_{72} & cpf_{73} & cpf_{74} & cpf_{75} & cpf_{76} \\ cpf_{81} & cpf_{82} & cpf_{83} & cpf_{84} & cpf_{85} & cpf_{86} \\ cpf_{91} & cpf_{92} & cpf_{93} & cpf_{94} & cpf_{95} & cpf_{96} \\ cpf_{101} & cpf_{102} & cpf_{103} & cpf_{104} & cpf_{105} & cpf_{106} \end{bmatrix} \quad (50)$$

Fig. 13 shows the outcome of experimental tests conducted on the proposed method in the IEEE 118-bus test system within a real time bidding power market environment and subjected to cyber-attacks. As shown in Figs 13a to 13c, the proposed approach effectively mitigates false data injection attacks while concurrently managing system uncertainties, ensuring the stabilization of power system frequency within permissible limits with a rapid response. Fig. 13d illustrates the rapid convergence to the sliding surface, leading to fast performance of the proposed method. The experimental results shown in Figs. 10 and 13 validate the effectiveness of the proposed method. This efficacy can be attributed to several critical factors expounded upon in the previous descriptions. The method's adeptness in managing various scenarios, encompassing unexpected challenges such as load variations, false data cyber-attacks, and system uncertainties, significantly contributes to its effectiveness. This adaptability ensures robustness and stability across diverse conditions. Furthermore, by actively mitigating cyber-attacks, generating accurate reference points, and guaranteeing finite-time convergence, the method showcases a swift and accurate response to dynamic changes. This capability plays a pivotal role in maintaining system frequency stability.

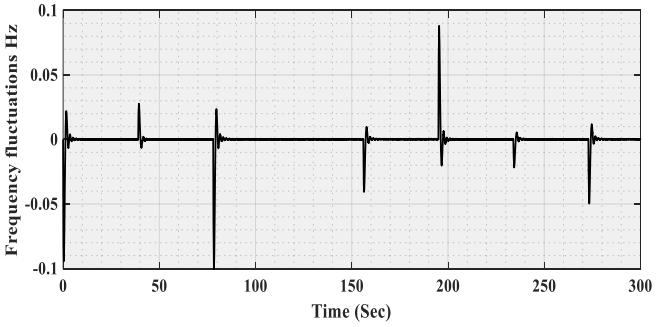

(a) Area 1

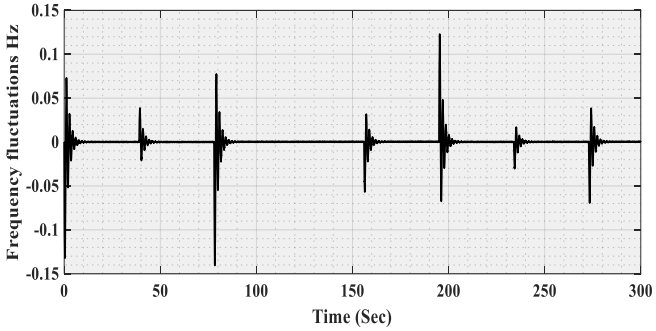

(b) Area 2

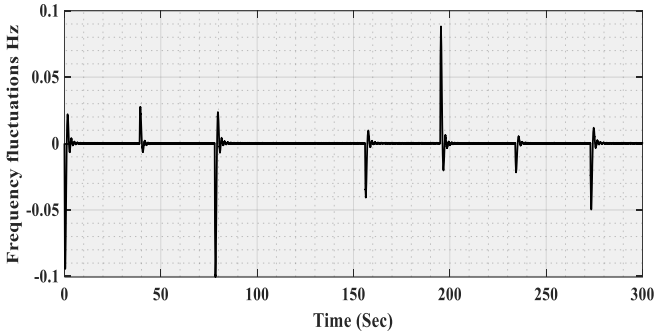

(c) Area 3

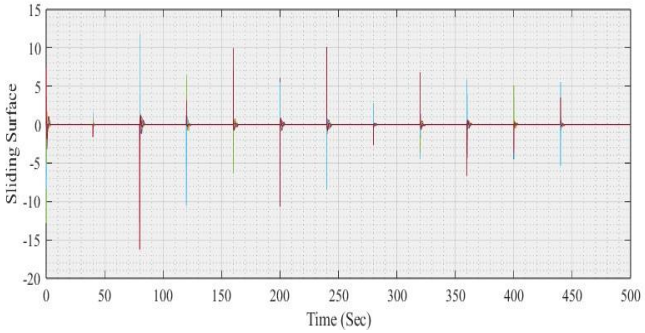

(d) Sliding surface convergence

Fig. 13. Experimental results of an IEEE 118-bus test system using the proposed method.

V. Conclusions

A new aspect of the real-time bidding market, focusing on the real time interactions between GENCOs and DISCOs, which was facilitated by the secondary hierarchical control layer within the smart power system, was investigated. Then, to address the challenges of smart grids within a real-time bidding market environment, a novel approach was proposed. This method employs an adaptive barrier-function-based second order sliding mode control, designed to be chatter-free, in order to counteract FDIA against supervisory control and data acquisition systems. The approach accommodates nonlinearities within the system, uncertainties in system parameters, and external disturbances. Test results of two modified renewable IEEE 39-bus and 118-bus test systems were presented to ensure and demonstrate the performance of the proposed method. These tests considered factors such as governor dead band and communication delays within the real-time bidding market environment. Test results have shown that the designed second order PID sliding surface in the proposed method creates strong robustness against both matched and unmatched conditions where false data cyber-attacks and load variations as well as system uncertainties and faults are considered. In addition, the finite time error trajectory tracking feature with the designed adaptive barrier function helps to

diminish the convergence area, limit the tracking error states in that area, and guarantee convergence at a finite time, which results in fast and exact fluctuations tracking. Therefore, the method can robustly reject FDIA while concurrently handling parametric uncertainties, as well as both matched and unmatched internal and external disturbances within the power bidding market, which results in the correct reference points simultaneously with cyber-attack rejection for maintaining system frequency stability. The proposed method effectively mitigates the chattering phenomenon and enhances convergence speed to render it suitable for real-time FDIA rejection and broader industrial applications. The simulation and experimental results, alongside comparison with conventional methods, validate the performance of the proposed method.

Appendix A

This appendix provides the proof stability for ***Condition (I):*** $\mathbf{0 < t \le \bar{t}}$

Proof: Considering the positive-definite Lyapunov function as

$$W(s_e(t), \dot{s_e}(t), k_{s_a}(t)) = 0.5\big(s_e(t)^2 + \dot{s_e}(t)^2 + \varphi^{-1}(k_{s_a}(t) - k_s)^2\big) \tag{A.1}$$

where φ is a positive scalar, and k_s is an unknown positive factor. The time-derivative of the above function gives

$$\dot{W}\left(s_e(t), \dot{s_e}(t), k_{s_a}(t)\right) = s_e(t)\dot{s_e}(t) + \dot{s_e}(t)\ddot{s_e}(t) + \varphi^{-1}(k_{s_a}(t) - k_s)\dot{k}_{s_a}(t) \tag{A.2}$$

Using (36), gives

$$\begin{aligned}\dot{W}\left(s_e(t), \dot{s_e}(t), k_{s_a}(t)\right) &= s_e(t)\dot{s_e}(t) + \varphi^{-1}(k_{s_a}(t) - k_s)\dot{k}_{s_a}(t) + \dot{s_e}(t)\big\{k_pC\big(Ax(t) + \xi Bu(t)\big) + k_pM(t) - k_p\dot{r}(t) + k_ie(t) + k_dCA\big(Ax(t) + \xi Bu(t)\big) + \xi k_dCB\dot{u}(t) + k_dN(t) - k_d\ddot{r}(t) - \beta\dot{s_e}(t)\big\}\end{aligned} \tag{A.3}$$

Substituting (47) into (A.3) gives

$$\begin{aligned}\dot{W}\left(s_e(t), \dot{s_e}(t), k_{s_a}(t)\right) &= s_e(t)\dot{s_e}(t) + \big\{k_dN(t) + k_pM(t) - (k_d\lambda|s_e(t)| + k_dk_{s_a}(t))\, sgn(\dot{s_e}(t))\big\}\dot{s_e}(t) + \ell\varphi^{-1}(k_{s_a}(t) - k_s)|\dot{s_e}(t)| \le \\ &-k_dk_{s_a}(t)\dot{s_e}(t)\, sgn(\dot{s_e}(t)) + \big\{k_d|N(t)| + k_p|M(t)| - (k_d\lambda - 1)|s_e(t)|\big\}|\dot{s_e}(t)| + \ell\varphi^{-1}(k_{s_a}(t) - k_s)|\dot{s_e}(t)| \le \\ &-(k_dk_s - k_d|N(t)| - k_p|M(t)| + (k_d\lambda - 1)|s_e(t)|)|\dot{s_e}(t)| - (k_d - \ell\varphi^{-1})\big(k_{s_a}(t) - k_s\big)|\dot{s_e}(t)|\end{aligned} \tag{A.4}$$

where since $k_s > |N(t)| + k_p|M(t)|/k_d$ and $\ell\varphi^{-1} < k_d$. Then (A.4) is expressed as

$$\begin{aligned}\dot{W}\left(s_e(t), \dot{s_e}(t), k_{s_a}(t)\right) &\le -2^{1/2}(k_d\lambda - 1)|\dot{s_e}(t)|\tfrac{|s_e(t)|}{2^{1/2}} - 2^{1/2}(k_dk_s - k_d|N(t)| - k_p|M(t)|)\tfrac{|\dot{s_e}(t)|}{2^{1/2}} - (2\varphi)^{1/2}(k_d - \ell\varphi^{-1})|\dot{s_e}(t)|\tfrac{k_{s_a}(t) - k_s}{(2\varphi)^{1/2}} \le -2^{1/2}\, min\big\{(k_d\lambda - 1)|\dot{s_e}(t)|, k_dk_s - k_d|N(t)| - k_p|M(t)|, (\varphi)^{1/2}(k_d - \ell\varphi^{-1})|\dot{s_e}(t)|\big\}\Big(\tfrac{|s_e(t)|}{2^{1/2}} + \tfrac{|\dot{s_e}(t)|}{2^{1/2}} + \tfrac{|k_{s_a}(t) - k_s|}{(2\varphi)^{1/2}}\Big) \le \\ &-\Phi W\left(s_e(t), \dot{s_e}(t), k_{s_a}(t)\right)^{1/2}\end{aligned} \tag{A.5}$$

where $\Phi = 2^{1/2}\, min\big\{(k_d\lambda - 1)|\dot{s_e}(t)|, k_dk_s - k_dN_{max} - k_pM_{max}, (\varphi)^{1/2}(k_d - \ell\varphi^{-1})|\dot{s_e}(t)|\big\}$. □

Appendix B

This appendix provides the proof stability for ***Condition (II):*** $\boldsymbol{t > \bar{t}}$

Proof: Constructing the positive-definite Lyapunov function as

$$Z\left(s_e(t), \dot{s_e}(t), k_{s_{psb}}(t)\right) = 0.5\left(s_e(t)^2 + \dot{s_e}(t)^2 + k_{s_{psb}}(t)^2\right) \tag{B.15 0}$$

where differentiating the Lyapunov function gives

$$\begin{aligned}\dot{Z}\left(s_e(t), \dot{s_e}(t), k_{s_{psb}}(t)\right) &= s_e(t)\dot{s_e}(t) + k_{s_{psb}}(t)\dot{k}_{s_{psb}}(t) + \dot{s_e}(t)\big\{k_pC\big(Ax(t) + \xi Bu(t)\big) + k_pM(t) - k_p\dot{r}(t) + k_ie(t) + k_dCA\big(Ax(t) + \xi Bu(t)\big) + \xi k_dCB\dot{u}(t) + k_dN(t) - k_d\ddot{r}(t) - \beta\dot{s_e}(t)\big\}\end{aligned} \tag{B.2}$$

Substituting (48) into (B.2) finds

$$\begin{aligned}&\dot{Z}\left(s_e(t), \dot{s_e}(t), k_{s_{psb}}(t)\right) \\ &= k_{s_{psb}}(t)\frac{\varepsilon}{(\varepsilon - |\dot{s_e}(t)|)^2}sign(\dot{s_e}(t))\big\{k_dN(t) + k_pM(t) - k_d\lambda s_e(t) - k_dk_{s_{psb}}(t)\, sgn(\dot{s_e}(t))\big\} + s_e(t)\dot{s_e}(t) \\ &+ \big\{k_dN(t) + k_pM(t) - k_d\lambda|s_e(t)|sgn(\dot{s_e}(t)) - k_dk_{s_{psb}}(t)\, sgn(\dot{s_e}(t))\big\}\dot{s_e}(t) \\ &\le -k_dk_{s_{psb}}(t)|\dot{s_e}(t)| + \big(k_d|N(t)| + k_p|M(t)|\big)|\dot{s_e}(t)| - (k_d\lambda - 1)|s_e(t)||\dot{s_e}(t)| \\ &+ k_{s_{psb}}(t)\frac{\varepsilon}{(\varepsilon - |\dot{s_e}(t)|)^2}sign(\dot{s_e}(t))\big\{k_dN(t) + k_pM(t) - k_d\lambda s(t) - k_dk_{s_{psb}}(t)\, sgn(\dot{s_e}(t))\big\} \\ &\le -\big(k_dk_{s_{psb}}(t) - k_d|N(t)| - k_p|M(t)|\big)|\dot{s_e}(t)| - (k_d\lambda - 1)|\dot{s_e}(t)||s_e(t)| \\ &- \frac{\varepsilon}{(\varepsilon - |\dot{s_e}(t)|)^2}\big\{k_dk_{s_{psb}}(t) - k_d|N(t)| - k_p|M(t)|\big\}k_{s_{psb}}(t)\end{aligned} \tag{B.3}$$

where since $k_{s_{psb}}(t) > |N(t)| + k_p|M(t)|/k_d$ and $\frac{\varepsilon}{(\varepsilon - |\sigma(t)|)^2} > 0$, we attain

$$\begin{aligned}\dot{Z}\left(s_e(t), \dot{s_e}(t), k_{s_{psb}}(t)\right) &\le -2^{1/2}(k_d\lambda - 1)|\dot{s_e}(t)|\tfrac{|s_e(t)|}{2^{1/2}} - 2^{1/2}\big(k_dk_{s_{psb}}(t) - k_d|N(t)| - k_p|M(t)|\big)\tfrac{|\dot{s_e}(t)|}{2^{1/2}} - \tfrac{2^{1/2}\,\varepsilon}{(\varepsilon - |\dot{s_e}(t)|)^2}\big\{k_dk_{s_{psb}}(t) - k_d|N(t)| - k_p|M(t)|\big\}\tfrac{k_{s_{psb}}(t)}{2^{1/2}} \le -2^{1/2}\, min\Big\{(k_d\lambda - 1)|\dot{s_e}(t)|, \big(k_dk_{s_{psb}}(t) - k_dN_{max} - k_pM_{max}\big)\Big[1, \tfrac{\varepsilon}{(\varepsilon - |\sigma(t)|)^2}\Big]\Big\}\Big(\tfrac{|s_e(t)|}{2^{1/2}} + \tfrac{|\dot{s_e}(t)|}{2^{1/2}} + \tfrac{k_{s_{psb}}(t)}{2^{1/2}}\Big) \le \\ &-\Gamma\, Z\left(s_e(t), \dot{s_e}(t), k_{s_{psb}}(t)\right)^{1/2}\end{aligned} \tag{B.4}$$

where $\Gamma = 2^{1/2}\, min\Big\{(k_d\lambda - 1)|\dot{s_e}(t)|, \big(k_dk_{s_{psb}}(t) - k_dN_{max} - k_pM_{max}\big)\Big[1, \frac{\varepsilon}{(\varepsilon - |\sigma(t)|)^2}\Big]\Big\}$. □

References

[1] J. Kumar, K.-H. Ng, and G. Sheble, "AGC simulator for price-based operation. II. Case study results," *IEEE Transactions on Power Systems*, vol. 12, no. 2, pp. 533-538, 1997.

[2] V. Donde, M. Pai, and I. A. Hiskens, "Simulation and optimization in an AGC system after deregulation," *IEEE transactions on power systems*, vol. 16, no. 3, pp. 481-489, 2001.

[3] P. Chen, D. Zhang, L. Yu, and H. Yan, "Dynamic event-triggered output feedback control for load frequency control in power systems with multiple cyber attacks," *IEEE Transactions on Systems, Man, and Cybernetics: Systems*, vol. 52, no. 10, pp. 6246-6258, 2022.

[4] C. Peng, H. Sun, M. Yang, and Y.-L. Wang, "A survey on security communication and control for smart grids under malicious cyber attacks," *IEEE Transactions on Systems, Man, and Cybernetics: Systems*, vol. 49, no. 8, pp. 1554-1569, 2019.

[5] A. Volkova, M. Niedermeier, R. Basmadjian, H. de Meer, and Tutorials, "Security challenges in control network protocols: A survey," *IEEE Communications Surveys*, vol. 21, no. 1, pp. 619-639, 2018.

[6] R. Schlegel, S. Obermeier, and J. Schneider, "A security evaluation of IEC 62351," (in English), *Journal of Information Security and Applications*, vol. 34, pp. 197-204, Jun 2017, doi: 10.1016/j.jisa.2016.05.007.

[7] L. Xie, Y. Mo, and B. Sinopoli, "Integrity Data Attacks in Power Market Operations," *IEEE Transactions on Smart Grid*, vol. 2, no. 4, pp. 659-666, 2011, doi: 10.1109/TSG.2011.2161892.

[8] Q. Zhang, F. Li, Q. Shi, K. Tomsovic, J. Sun, and L. Ren, "Profit-Oriented False Data Injection on Electricity Market: Reviews, Analyses, and Insights," *IEEE Transactions on Industrial Informatics*, vol. 17, no. 9, pp. 5876-5886, 2021, doi: 10.1109/TII.2020.3036104.

[9] J. P. Farwell and R. Rohozinski, "Stuxnet and the Future of Cyber War," *Survival*, vol. 53, no. 1, pp. 23-40, 2011.

[10] D. U. J. E. I. S. Case and A. Center, "Analysis of the cyber attack on the Ukrainian power grid," vol. 388, no. 1-29, p. 3, 2016.

[11] S. D. Roy and S. Debbarma, "Detection and Mitigation of Cyber-Attacks on AGC Systems of Low Inertia Power Grid," *IEEE Systems Journal*, vol. 14, no. 2, pp. 2023-2031, 2020, doi: 10.1109/JSYST.2019.2943921.

[12] H. Xu, Y. Lin, X. Zhang, and F. Wang, "Power System Parameter Attack for Financial Profits in Electricity Markets," *IEEE Transactions on Smart Grid*, vol. 11, no. 4, pp. 3438-3446, 2020, doi: 10.1109/TSG.2020.2977088.

[13] G. Liang, S. R. Weller, F. Luo, J. Zhao, and Z. Y. Dong, "Generalized FDIA-Based Cyber Topology Attack With Application to the Australian Electricity Market Trading Mechanism," *IEEE Transactions on Smart Grid*, vol. 9, no. 4, pp. 3820-3829, 2018, doi: 10.1109/TSG.2017.2677911.

[14] K. Jhala, B. Natarajan, A. Pahwa, and H. Wu, "Stability of Transactive Energy Market-Based Power Distribution System Under Data Integrity Attack," *IEEE Transactions on Industrial Informatics*, vol. 15, no. 10, pp. 5541-5550, 2019, doi: 10.1109/TII.2019.2901768.

[15] Q. Zhang and F. Li, "Cyber-Vulnerability Analysis for Real-Time Power Market Operation," *IEEE Transactions on Smart Grid*, vol. 12, no. 4, pp. 3527-3537, 2021, doi: 10.1109/TSG.2021.3066398.

[16] H. Bevrani, *Robust power system frequency control*. Springer, 2014.

[17] S. H. Rouhani, H. Mojallali, and A. Baghramian, "An optimized fuzzy sliding based active disturbance rejection control for simultaneous cyber-attack tolerant and demand response participation program," *International Transactions on Electrical Energy Systems*, vol. 31, no. 12, p. e13206, 2021.

[18] Z. Cheng, S. Hu, D. Yue, C. Dou, and S. Shen, "Resilient Distributed Coordination Control of Multiarea Power Systems Under Hybrid Attacks," *IEEE Transactions on Systems, Man, and Cybernetics: Systems*, vol. 52, no. 1, pp. 7-18, 2022, doi: 10.1109/TSMC.2021.3049373.

[19] P. Chen, D. Zhang, L. Yu, and H. Yan, "Dynamic Event-Triggered Output Feedback Control for Load Frequency Control in Power Systems With Multiple Cyber Attacks," *IEEE Transactions on Systems, Man, and Cybernetics: Systems*, vol. 52, no. 10, pp. 6246-6258, 2022.

[20] Y. Liu, Y. Chen, and M. Li, "Dynamic event-based model predictive load frequency control for power systems under cyber attacks," *IEEE Transactions on Smart Grid*, vol. 12, no. 1, pp. 715-725, 2020.

[21] X. Liu, D. Bai, S. Qiao, G. Xiao, and S. S. Ge, "Resilient and event-triggered sliding mode load frequency control for multi-area power systems under hybrid cyber attacks," *IET Control Theory & Applications*, vol. 16, no. 17, pp. 1739-1750, 2022.

[22] J. Liu, Y. Gu, L. Zha, Y. Liu, and J. Cao, "Event-Triggered H∞ Load Frequency Control for Multiarea Power Systems Under Hybrid Cyber Attacks," *IEEE Transactions on Systems, Man, and Cybernetics: Systems*, vol. 49, no. 8, pp. 1665-1678, 2019, doi: 10.1109/tsmc.2019.2895060.

[23] J. Wang, D. Wang, L. Su, J. H. Park, and H. Shen, "Dynamic Event-Triggered H∞ Load Frequency Control for Multi-Area Power Systems Subject to Hybrid Cyber Attacks," *IEEE Transactions on Systems, Man, and Cybernetics: Systems*, vol. 52, no. 12, pp. 7787-7798, 2022.

[24] Z. Hu, S. Liu, W. Luo, and L. Wu, "Resilient distributed fuzzy load frequency regulation for power systems under cross-layer random denial-of-service attacks," *IEEE Transactions on Cybernetics*, vol. 52, no. 4, pp. 2396-2406, April 2022, doi: 10.1109/TCYB.2020.3005283.

[25] S. H. Rouhani, E. Abbaszadeh, M. A. Sepestanaki, S. Mobayen, C. L. Su, and A. Nemati, "Adaptive Finite-Time Tracking Control of Fractional Microgrids Against Time-Delay Attacks," *IEEE Transactions on Industry Applications*, pp. 1-13, 2023, doi: 10.1109/TIA.2023.3312223.

[26] A. Nemati, M. Peimani, S. Mobayen, and S. Sayyedfattahi, "Adaptive non-singular finite time control of nonlinear disturbed cyber-physical systems with actuator cyber-attacks and time-varying delays," *Information Sciences*, vol. 612, pp. 1111-1126, Oct 2022.

[27] Z. Y. Zuo, "Non-singular fixed-time terminal sliding mode control of non-linear systems," *IET Control Theory A*, vol. 9, no. 4, pp. 545-552, Feb 26 2015, doi: 10.1049/iet-cta.2014.0202.

[28] I. Eker, "Second-order sliding mode control with experimental application," *ISA Trans*, vol. 49, no. 3, pp. 394-405, Jul 2010.

[29] Z. Cao, Y. Niu, and J. Song, "Finite-Time Sliding-Mode Control of Markovian Jump Cyber-Physical Systems Against Randomly Occurring Injection Attacks," *IEEE Transactions on Automatic Control*, vol. 65, no. 3, pp. 1264-1271, 2020, doi: 10.1109/TAC.2019.2926156.

[30] X. X. Lv, Y. H. Sun, W. Q. Hu, and V. Dinavahi, "Robust load frequency control for networked power system with renewable energy via fractional-order global sliding mode control," *IET Renewable Power Generation*, vol. 15, no. 5, pp. 1046-1057, Apr 2021, doi: 10.1049/rpg2.12088.

[31] J. Hu, H. X. Zhang, H. J. Liu, and X. Y. Yu, "A survey on sliding mode control for networked control systems," *International Journal of Systems Science*, vol. 52, no. 6, pp. 1129-1147, Apr 26 2021.

[32] I. Boiko, L. Fridman, A. Pisano, and E. Usai, "Analysis of Chattering in Systems With Second-Order Sliding Modes," *IEEE Transactions on Automatic Control*, vol. 52, no. 11, pp. 2085-2102, 2007.

[33] M. N. Aydin and R. Coban, "PID sliding surface-based adaptive dynamic second-order fault-tolerant sliding mode control design and experimental application to an electromechanical system," *International Journal of Control*, vol. 95, no. 7, pp. 1767-1776, 2021.

[34] H. L. N. N. Thanh and S. K. Hong, "Quadcopter Robust Adaptive Second Order Sliding Mode Control Based on PID Sliding Surface," *IEEE Access*, vol. 6, pp. 66850-66860, 2018, doi: 10.1109/ACCESS.2018.2877795.

[35] M. Van, "Higher-order terminal sliding mode controller for fault accommodation of Lipschitz second-order nonlinear systems using fuzzy neural network," *Applied Soft Computing*, vol. 104, p. 107186, 2021.

[36] H. B. Sun, S. H. Li, and C. Y. Sun, "Finite time integral sliding mode control of hypersonic vehicles," *Nonlinear Dynamics*, vol. 73, no. 1-2, pp. 229-244, Jul 2013, doi: 10.1007/s11071-013-0780-4.

[37] S. Laghrouche, M. Harmouche, Y. Chitour, H. Obeid, and L. M. Fridman, "Barrier function-based adaptive higher order sliding mode controllers," *Automatica*, vol. 123, p. 109355, Jan 2021.

[38] H. Obeid, L. M. Fridman, S. Laghrouche, and M. Harmouche, "Barrier function-based adaptive sliding mode control," *Automatica*, vol. 93, pp. 540-544, Jul 2018, doi: 10.1016/j.automatica.2018.03.078.

[39] H. Obeid, S. Laghrouche, L. Fridman, Y. Chitour, and M. Harmouche, "Barrier Function-Based Adaptive Super-Twisting Controller," *IEEE Transactions on Automatic Control*, vol. 65, no. 11, pp. 4928-4933, 2020.

[40] J. Kumar, K.-H. Ng, and G. Sheble, "AGC simulator for price-based operation. I. A model," *IEEE Transactions on Power Systems*, vol. 12, no. 2, pp. 527-532, 1997.

[41] J. Kacprzyk, "Lecture notes in networks and systems," ed: Springer, 2019.

[42] S. H. Rouhani, H. Mojallali, and A. Baghramian, "Load frequency control in the presence of simultaneous cyber-attack and participation of demand response program," *Transactions of the Institute of Measurement and Control*, vol. 44, no. 10, pp. 1993-2011, Jun 2022.

[43] A. Ameli, A. Hooshyar, E. F. El-Saadany, and A. M. Youssef, "Attack Detection and Identification for Automatic Generation Control Systems," *IEEE Transactions on Power Systems*, vol. 33, no. 5, pp. 4760-4774, 2018.

[44] O. Mofid, S. Mobayen, C. Zhang, and B. Esakki, "Desired tracking of delayed quadrotor UAV under model uncertainty and wind disturbance using adaptive super-twisting terminal sliding mode control," *ISA Transactions*, vol. 123, pp. 455-471, 2022, doi: https://doi.org/10.1016/j.isatra.2021.06.002.

[45] L. V. Suresh Kumar, G. V. Nagesh Kumar, and S. Madichetty, "Pattern search algorithm based automatic online parameter estimation for AGC with effects of wind power," *International Journal of Electrical Power & Energy Systems*, vol. 84, pp. 135-142, 2017, doi: 10.1016/j.ijepes.2016.05.009.

[46] J. Han, "From PID to Active Disturbance Rejection Control," *IEEE Transactions on Industrial Electronics*, vol. 56, no. 3, pp. 900-906, 2009.

[47] A. Delavari, P. Brunelle, and I. Kamwa, "Real-time Closed-loop PQ Control of NPC Multi-level Converter Using OPAL-RT and Speedgoat Simulators," in *2018 IEEE Electrical Power and Energy Conference (EPEC)*, 10-11 Oct. 2018 2018, pp. 1-5, doi: 10.1109/EPEC.2018.8598323.

[48] S. Carpiuc, M. Schiesser, and C. Villegas, "Current Control and FPGA–Based Real–Time Simulation of Grid–Tied Inverters," in *2020 22nd European Conference on Power Electronics and Applications (EPE'20 ECCE Europe)*, 7-11 Sept. 2020, pp. P.1-P.7.